Changing phytoplankton phenology in the marginal ice zone west of the Antarctic Peninsula

Running page head: Changing phenology of polar phytoplankton

Authors and addresses:

Jessica S. Turner[1*], Heidi Dierssen[1], Oscar Schofield[2], Heather H. Kim[3], Sharon Stammerjohn[4], David R. Munro[4,5], and Maria Kavanaugh[6]

[1] Department of Marine Sciences, University of Connecticut, Groton, CT, 06340, USA.
[2] Department of Marine and Coastal Sciences, Rutgers University, NJ, 08854, USA.
[3] Department of Marine Chemistry and Geochemistry, Woods Hole Oceanographic Institution, Woods Hole, MA, 02453, USA.
[4] Cooperative Institute for Research in Environmental Sciences, University of Colorado, Boulder, CO, 80309, USA.
[5] National Oceanic and Atmospheric Administration, Global Monitoring Laboratory, Boulder, CO, 80309, USA.
[6] College of Earth, Ocean, and Atmospheric Sciences, Oregon State University, Corvallis, OR, 97331, USA.

ABSTRACT: Climate change is altering global ocean phenology, the timing of annually occurring biological events. We examined the changing phenology of the phytoplankton accumulation season west of the Antarctic Peninsula to show that blooms are shifting later in the season over time in ice-associated waters. The timing of the start date and peak date of the phytoplankton accumulation season are occurring later over time from 1997 to 2022 in the marginal ice zone and over the continental shelf. A divergence is seen between offshore waters and ice-associated waters, with offshore bloom timing becoming earlier, yet marginal ice zone and continental shelf bloom timing shifting later. Higher chlorophyll-a concentration (Chl-a) in the fall season is seen in recent years, especially over the northern continental shelf. Minimal long-term trends in annual Chl-a occurred, likely due to the combination of later start dates in spring and higher Chl-a in fall. The most likely mechanism for later spring start dates is increasing spring wind speed, leading to deeper wind mixing in a region experiencing sea ice loss. Later phytoplankton bloom timing over the marginal ice zone and continental shelf will have consequences for surface ocean carbon uptake, food web dynamics, and trophic cascade.

KEY WORDS: Phenology; Antarctic ecology; Remote sensing; Marginal Ice Zone; Chlorophyll-a; Polar regions; Phytoplankton blooms; Satellite data

[*] Corresponding author, email: jturner@uconn.edu

1. INTRODUCTION

Phenology involves the timing of annually recurring events in nature. For ocean ecosystems, a prominent annual event is the start date of the phytoplankton accumulation season, commonly referred to as the start of the spring bloom. In this paper, we use the term "accumulation season" to describe the period during each year when phytoplankton biomass as measured by surface chlorophyll-a (Chl-a) concentration is increasing, such that the average phytoplankton mass-specific loss rates are smaller than their growth rates. The spring bloom is the foundation of the marine food web. The intense seasonal surge of primary production supports the zooplankton community, which in turn provides a rich food source for fish and other higher trophic level organisms (Riley 1942, Fenchel 1988, Winder & Sommer 2012). As climate warms, most research predicts earlier start dates for the phytoplankton accumulation season in the world's oceans. On average, studies show a shift toward earlier phytoplankton bloom timing by approximately four days per decade (Poloczanska et al. 2013, 2016, IPCC 2019). Satellite remote sensing of global phytoplankton blooms similarly suggests that the phytoplankton accumulation season is starting earlier and lasting longer (Friedland et al. 2018).

High latitude polar ecosystems are often treated as a single entity in global studies of phytoplankton phenology characterized by short-duration, high-intensity summer phytoplankton blooms (Racault et al. 2012). Satellite-derived Chl-a in the Southern Ocean reveals increasing trends over time in offshore open ocean waters in most sectors (Del Castillo et al. 2019, Pinkerton et al. 2021). Indeed, the IPCC (2019) summarizes with "high confidence" that changes in polar sea ice and ocean stratification are occurring, causing changes in the "timing, duration, and intensity of primary production." In a warming climate, start dates of the phytoplankton

accumulation season at high latitudes are predicted to shift earlier by about five days per decade (Friedland et al. 2018, Henson et al. 2018).

However, polar seas with seasonal sea ice experience more variability than the broad high-latitude regions examined in global phenology modeling studies. The Marginal Ice Zone (MIZ) experiences the highest seasonal variability in sea ice cover for a given polar region (Tréguer & Jacques 1992). In Antarctic waters, the MIZ comprises ~6 million km^2 of about 19 million km^2 of total Antarctic sea-ice cover (32%) and makes up a majority of the sea ice cover for the WAP region (~60%) (Stroeve et al. 2016, Vichi 2022). Sea ice variability in the MIZ is linked to variability in phytoplankton and krill populations, thus this region plays an important role in supporting the marine ecosystem throughout many trophic levels. The MIZ surrounding Antarctica experiences some of the highest winds and waves on the planet, and it is here where the timing of sea ice retreat and advance, light availability, wind-driven mixing, bathymetric effects on mixing, and nutrient supply are highly variable over both space and time. Changes such as increased wind-driven mixing resulting in reduced stratification early in the season can shift the timing of the start date of the phytoplankton accumulation season later in the year, a scenario which has been observed in other polar seas with seasonal sea ice (Stabeno et al. 2001, 2012).

In this paper, we explore the seasonal phenology of phytoplankton biomass at a sentinel region for polar ecosystem change: the marine system of the West Antarctic Peninsula (WAP) (Henley et al. 2019). The WAP is often used as a case study for changing polar systems due to its declining seasonal sea ice, melting of nearby glaciers, exposure to high circumpolar winds, currents and waves, a dynamic food web, and regionally relevant sinks for anthropogenic CO_2 (Arrigo et al. 2008, Henley et al. 2019). The WAP region is governed by the seasonal presence

of sea ice, whose dynamics are driven by multiple climatic forcings (Stammerjohn et al. 2008, Meredith et al. 2017, 2021). High Chl-a concentrations at the surface depend in part on low wind speeds (Saba et al. 2014), as deeper mixing may result in both dilution and light limitation. Each spring season, sea ice melt leads to stratification, which allows for initiation of the phytoplankton accumulation season (Moline 1998, Vernet et al. 2008, Carvalho et al. 2015, Schofield et al. 2018). Later in the summer season, glacial melt can also sustain or intensify coastal stratification, thus supporting or sustaining high phytoplankton biomass in surface waters (Dierssen et al. 2002, Meredith et al. 2021).

Most in situ observations in polar systems are collected during the summer, limiting knowledge of seasonal phenology. For example, January in situ observations show trends toward shallower summer mixed layer depths, increased summer primary production, and enhanced summer carbon drawdown along the WAP (Schofield et al. 2018, Brown et al. 2019). However, phytoplankton dynamics need to be examined throughout the polar season for a better understanding of ecosystem functions and carbon cycling. Such phenology analysis allows for the evaluation of climatological changes in polar regions and for predicting impacts on food web dynamics. Previous time series analyses along the WAP with high temporal coverage (Saba et al. 2014, Kim et al. 2018, e.g., Brown et al. 2019, Thibodeau et al. 2019, Cimino et al. 2023) are spatially limited to either the sampling grids of research vessels or point locations at coastal research stations. Satellite remote sensing of ocean color provides the means to study phytoplankton dynamics from September to April, with wide spatial coverage and a 25-year time series (1997 to 2022). Ocean color remote sensing is inherently limited by some factors, such as surface-only Chl-a estimates without depth-integrated biomass, Chl-a as an imperfect proxy for biomass, limited retrievals at high solar zenith angles, clouds, and the need to correct for

106 atmospheric and surface phenomena that interfere with estimates of water-leaving radiance.
107 Despite these limitations, remote sensing is an indispensable tool for ocean observing thanks to
108 increased spatial and temporal coverage in regions with limited accessibility such as western
109 Antarctica. Ocean color remote sensing in western Antarctica is useful for studying
110 phytoplankton rather than other optically-active constituents, since there are no major terrestrial
111 sources of sediments (Pan et al. 2019) or colored dissolved organic matter (Patterson 2000,
112 Norman et al. 2011). Ocean color data are useful for the WAP region from 1997 onward,
113 beginning with the SeaWiFS sensor. The earlier Coastal Zone Color Scanner (CZCS) (e.g.,
114 Montes-Hugo et al. 2009) is not appropriate for long-term analysis of polar regions, since spatial
115 coverage is limited to the northern WAP, limiting synoptic view of feature migration and
116 correlations with the migration of the seasonal sea ice margin (Fig. S1, S2 in the Supplement).
117 The objectives of this study are to 1) quantify the time series of satellite-derived surface
118 Chl-a up to recent years, 2) illustrate spatial gradients and temporal trends in Chl-a and its
119 seasonal timing, and 3) identify long-term shifts in the timing of phenological events in the
120 phytoplankton accumulation season along the WAP. Results show that the phytoplankton
121 accumulation season is starting and peaking later over time throughout much of the WAP region,
122 with decreased Chl-a in the spring season and increased Chl-a in the fall season in recent years.

123 # 2. METHODS

124 ## 2.1. Study area

125 The WAP region (-80°W to -55°W, -70°S to -60°S) was analyzed including both the
126 offshore and shelf environments. Five ecoregions were used: 1) the southern polar front (SPF),
127 the marginal ice zone (MIZ), the northern shelf, the mid shelf, and the southern shelf (Fig. 1).
128 The SPF corresponds to the Permanently Open Ocean Zone, which is considered an almost

129 oligotrophic ocean experiencing light limitation due to high wind mixing and nutrient limitation
130 (Jeandel et al. 1998). The MIZ is influenced by the receding ice edge each spring and advancing
131 ice edge each fall, and this ecoregion is more productive than the Permanently Open Ocean Zone
132 but not as productive as the shelf and coast (Tréguer & Jacques 1992). The shelf, sometimes
133 labeled the Coastal and Continental Shelf Zone, is considered the most highly productive region
134 of the Southern Ocean, with large blooms occurring over the course of the phytoplankton
135 accumulation season (Arrigo & McClain 1994, Smith et al. 1996, Dierssen et al. 2000). We
136 further divide the shelf into three ecoregions from north to south based on the phenology of
137 bloom timing and seasonal sea ice retreat (Fig. 1). Thus, ecoregions correspond to both
138 bathymetric gradients (i.e., shelf vs. off-shelf) and the spatial gradients in the mean timing of
139 bloom start dates. The line between the SPF and the MIZ approximately corresponds to both the
140 northern limit of the sea ice zone and the Antarctic Circumpolar Current's southern boundary,
141 known as the southern Antarctic Circumpolar Current front (Orsi et al. 1995, Martinson 2012,
142 Chapman et al. 2020).

143 **2.2. Satellite ocean color data**

144 2.2.1. Satellite-derived Chl-a

145 Satellite-derived Chl-a data were sourced from CMEMS GlobColour (Garnesson et al.
146 2019). This product is a merged multi-sensor dataset using Chl-a data from SeaWiFS (1997-
147 2010), MODIS-Terra (2000-present), MODIS-Aqua (2002-present), MERIS (2002-2012),
148 VIIRS-NPP (2012-present), VIIRS-NOAA20 (2018-present), OLCI-S3A (2016-present) and
149 OLCI-S3B (2018-present), processed to a common spatial resolution of 4 km. Chl-a from this
150 record is a daily interpolated gap-filled Level-4 data product, flagged and processed as in
151 Garnesson et al. (2019). Gap-filled and non-gap-filled Chl-a concentrations were consistent with

one another in the WAP region over the time series analyzed in this study (Fig. S3 in the Supplement). The Chl-a algorithm in this dataset is a global algorithm based on the tendency of phytoplankton to absorb comparatively more blue light relative to green (Gohin et al. 2002, Hu et al. 2012, Garnesson et al. 2019). Merging of data from multiple sensors created some inconsistencies in the time series due to the addition of higher spatial resolution sensors such as MERIS and OLCI in later years (Van Oostende et al., 2022). However, most of those inconsistencies occur in very nearshore waters due to the enhanced ability of the added sensors to observe specific geographical pixels. This dataset is suitable for our analysis thanks to the broad spatial coverage of the ecoregions in this study, including mostly offshore waters not impacted by the addition of higher spatial resolution sensors.

Global Chl-a algorithms are known to underestimate in situ Chl-a in the WAP region by a factor of 2 to 2.5 due to a combination of pigment packaging, low particulate backscattering, and low concentrations of dissolved substances (Mitchell & Holm-Hansen 1991, Mitchell 1992, Dierssen 2000, Dierssen & Smith 2000, Kahru & Mitchell 2010, IOCCG 2015). To correct for the underestimation by global algorithms, we applied a 4^{th}-order polynomial to the global Chl-a dataset to match field data (Dierssen and Smith 2000). As shown in Fig. S4 and Fig. S5 in the Supplement, this correction is minimal at low Chl-a concentrations representative of offshore waters of the SPF, where the standard algorithms generally perform well (Dierssen 2000, Haëntjens et al. 2017). These corrections are conducted to better reflect the range in Chl-a from shelf to open ocean in the WAP region. Because phenology analysis depends on the relative Chl-a rather than absolute Chl-a, and because the correction is consistent throughout the satellite time series, it does not impact the analyses of Chl-a phenology over time.

The use of satellite-derived surface Chl-a as a tool to study phytoplankton dynamics is useful in polar regions despite some inherent limitations. Chl-a is an imperfect metric for phytoplankton biomass, since the ratio of Chl-a to biomass can vary with phytoplankton carbon, light, temperature, and nutrient concentrations (Cleveland et al. 1989, Babin et al. 1996, Geider et al. 1997, Barbieux et al. 2018). In some systems, Chl-a in the surface ocean may exhibit different patterns compared to vertically-integrated phytoplankton biomass throughout the water column, as seen in the North Atlantic (Boss & Behrenfeld 2010). The relationship between surface and depth-integrated Chl-a is generally well constrained in the WAP region (Dierssen et al. 2000).

2.2.2. Satellite data availability

Satellite data availability enables analysis over austral spring, summer, and early fall for areas that are generally free of sea ice during the summer season in most years (Fig. S6 in the Supplement). Available data are deemed accumulation season data since low light and under sea ice data are unavailable in austral winter. Data are available for the entire WAP region from September to April, partially unavailable in May and August, and completely unavailable in June and July due to low light and ice cover (Fig. 2 and Fig. S7 in the Supplement).

2.3. Environmental data

Long-term trends in environmental factors were analyzed in addition to Chl-a, including wind speed, photosynthetically active radiation (PAR), and sea surface temperature (SST). ERA5 reanalysis data were used to analyze trends in wind speed over time (C3S 2018). Hourly wind speeds were calculated from hourly u and v component velocities at 0.25° x 0.25° horizontal resolution at 10 meters above Earth's surface using $ws = sqrt(u^2+v^2)$. Hourly wind speeds were averaged to daily and monthly wind speeds. For wind, relevant data assimilated into the ERA

197 wind product include satellite observations (infrared and microwave radiances, retrievals from
198 radiance data, and scatterometer data) and in situ observations (ships, aircraft, buoys, radar, and
199 radiosondes). Due to the known low quantity of in situ data and low reliability of satellite
200 observations of the sea surface in the presence of seasonal sea ice, only ERA5 reanalysis data in
201 the offshore SPF ecoregion were analyzed (Fig. 1). PAR data were downloaded from NASA
202 ocean color web from SeaWiFS, MODIS-Terra, and MODIS-Aqua (Frouin & Pinker 1995,
203 Frouin et al. 2002, 2012) as a Level-3 daily product at 9 km spatial resolution. This dataset
204 provides an estimate of daily average PAR in Einstein m^{-2} d^{-1} based on observed top-of-
205 atmosphere radiances in in the 400-700 nm range that do not saturate over clouds. For years with
206 multiple sensors in orbit at once (i.e., SeaWiFS, MODIS-Terra, and MODIS-Aqua for years
207 2002-2010), PAR data from all sensors were averaged for each day to create one average
208 mapped file per day. Since PAR data from ocean color using this approach are only valid over
209 dark waters and are invalid over sea ice as a result of the plane-parallel algorithm, only PAR data
210 in the offshore SPF ecoregion were analyzed (Fig. 1). SST data were downloaded from the
211 Global Ocean OSTIA Sea Surface Temperature and Sea Ice Reprocessed dataset from CMEMS
212 as a Level-4 daily product at 0.05° x 0.05° horizontal resolution (Good et al. 2020).

213 **2.4. Data analysis**

214 2.4.1. Spatial and temporal boundaries of analysis

215 Spatially, analysis was performed only for ocean color data pixels where at least 30% of
216 daily data were present, which removed noise by excluding locations covered by seasonal sea ice
217 for the majority of the time series (Fig. S6 in the Supplement). Temporally, data were analyzed
218 by austral year, 1 July through 30 June, to encompass the entire southern hemisphere

accumulation season rather than the boreal calendar year. The dataset includes September 1997 through August 2022.

2.4.2. Phenology metrics

Analysis of changing timing of phytoplankton dynamics focused on the start date of the phytoplankton accumulation season, heretofore referred to as the "start date." In addition to the start date, we examined the "peak date," the timing of the maximum concentration of Chl-a. While global studies often use bloom duration as a metric of phytoplankton phenology (Racault et al. 2012, 2015, Friedland et al. 2018), the WAP region is unsuitable for the traditional definition of bloom duration. In many parts of the WAP, especially over the shelf, prolonged elevated Chl-a concentrations continue throughout the austral summer and fall (Kim et al. 2018). High Chl-a concentrations, while variable, can persist into the fall season up until low light and sea ice advance render satellite observations unusable. Thus, instead of duration, we focused on start date and peak date as the most suitable metrics. Each of these phenology metrics were calculated for each year in the 25-year record as day of austral year from 1 July to 30 June. The metrics start date and peak date were therefore truly temporally independent from year to year, representing individual annual values in units of day-of-year. Decadal trends were compared using the austral years (July to June) 2000-2001 through 2010-2011 versus 2011-2012 through 2021-2022. These sets of years were chosen based on change-point analysis for the start date and peak date time series for each region (Killick et al. 2012). Change-point analysis showed distinct change-points at the year 2012 for the MIZ, northern shelf, and mid shelf ecoregions (Fig. S8 and Fig. S9 in the Supplement).

2.4.3. Phenology metric sensitivity analysis

There are several different ways of looking at changes in the phenology of phytoplankton blooms (Brody et al. 2013, Thomalla et al. 2015). We tried multiple methods (Fig. S10 in the Supplement) and chose the Threshold approach, because it showed the clearest spatial gradient in the average timing of the start date across all years and fell in the middle of the distribution of all indices in terms of resulting trends over time (Fig. S10 in the Supplement). The Threshold approach defines the start of the phytoplankton accumulation season as the day when Chl-a becomes greater than the threshold value equal to the long-term median plus 5% (Siegel et al. 2002, Racault et al. 2012) and remains above that threshold value for 5 consecutive days.

For a given location in the waters west of the Antarctic Peninsula, a typical year begins with low Chl-a when satellite data first become available, then increases to a peak Chl-a value in mid-summer, then decreases with shortening day length and sea ice advance. However, some locations during some years experienced "no bloom" as defined by never exceeding 2.5 times the long-term threshold value (where the threshold value is the long-term median plus 5%, i.e., 0.4 mg m^{-3} for the mid shelf). Therefore, additional quality control was performed by removing years without a substantial phytoplankton bloom from all phenology analyses. This quality control measure had only a small effect, since 19 of 25 years experienced a substantial bloom for > 90% of the ocean area analyzed, and even the year with the largest number of "no bloom" locations (1998) showed substantial blooms in 77% of pixels (Fig. S11 in the Supplement).

2.5. Statistical analysis

Time series analysis was performed for the WAP region as a whole using mapped long-term trends at each x,y pixel location and for separate ecoregions. Ecoregion time series were created by averaging the pixels (geometric mean) within the polygons shown in Fig. 1. For all statistical tests, we used a significance threshold of 0.05.

264 To determine the significance of decadal differences in the daily time series, we applied a
265 Kruskal-Wallis test, i.e., non-parametric ANOVA, *kruskalwallis* function in MATLAB 9.6.0
266 R2019a (The MathWorks Inc. 2019) to compare each day-of-year mean Chl-a for 2001-2011 to
267 the same day-of-year mean Chl-a for 2012-2022 in each ecoregion. The application of a non-
268 parametric test was appropriate since the distributions of decadal Chl-a by day-of-year (e.g., Chl-
269 a for December 1st in the northern shelf across all years in a given decade) were non-normal.
270 The null hypothesis is that both decades have the same center parameter for their distribution.
271 To assess the significance of decadal differences in start date and peak date by ecoregion,
272 we calculated the spatial mean of each metric in each ecoregion during each year to find the
273 decadal means and medians, then compared decadal medians using non-parametric Kruskal-
274 Wallis tests. Like the test above, the null hypothesis is that both decades have the same center
275 parameter for their distribution. The application of a non-parametric test was appropriate since
276 decadal start dates and peak dates by ecoregion (e.g., northern shelf mean start date across all
277 years in a given decade) were not normally distributed.
278 Mapped long-term trends in each phenology metric and in month-wise Chl-a were
279 calculated using Theil-Sen non-parametric estimates of slope over time (Gilbert 1987) at each
280 x,y location, using the *TheilSen* function in MATLAB R2019a (Danziger 2024). The statistical
281 significance of these mapped trends was tested at each x,y location using a non-parametric
282 Mann-Kendall test of monotonic trends (Mann 1945, Kendall 1975), with the Climate Data
283 Toolbox *mann_kendall* function in MATLAB R2019a (Greene et al. 2019). The application of a
284 non-parametric test was appropriate since the distributions of phenology metrics (e.g., start date
285 and peak date for all years) and month-wise Chl-a (e.g., October Chl-a for all years) were non-
286 normal. For mapped trends, the null hypothesis is that there is no trend in the data over time. No

287 detrending was performed on phenology metric time series, because as single day-of-year values,
288 these were considered independent data points from year to year. No detrending was performed
289 for month-wise Chl-a, as each month's mean Chl-a was considered an independent data point
290 from year to year (e.g., Fig. 9).

291 To determine trends by ecoregion, regionally averaged monthly Chl-a and phenology
292 metrics (one value per year) were tested for significant trends over time using a non-parametric
293 Theil-Sen slope test. Detrending was performed to de-seasonalize the overall long-term monthly
294 Chl-a time series (Fig. S12 in the Supplement) using the Climate Data Toolbox *deseason*
295 function in MATLAB R2019a (Greene et al. 2019), which detrends to isolate the seasonal
296 component, then subtracts the seasonal component of the time series from the original data (Fig.
297 S12 in the Supplement). No detrending was performed on phenology metric time series, because
298 as single day-of-year values, these were considered independent data points from year to year.
299 Theil-Sen non-parametric estimates of slope were performed on each ecoregion's de-
300 seasonalized Chl-a to calculate trends. The significance of the trends was assessed with Mann-
301 Kendall tests. The application of a non-parametric test was appropriate since both the de-
302 seasonalized monthly Chl-a (e.g., northern shelf mean Chl-a during every month over the entire
303 time series) and phenology metrics (e.g., northern shelf mean start date and peak date across all
304 years) were not normally distributed. Like the test above, the null hypothesis is that there is no
305 trend in the data over time.

306 For environmental data, month-wise trends over time and decadal comparisons followed
307 the same statistical methods used for Chl-a. For wind speed, long-term trends in month-wise
308 wind speed were calculated using Theil-Sen non-parametric estimates of slope over time at each
309 x,y location in m s^{-1} yr^{-1}. Each month's relative trend was calculated as the trend (m s^{-1} yr^{-1})

relative to the long-term mean wind speed (m s^{-1}) at each x,y location for each month. The significance of month-wise trends was assessed using Mann-Kendall tests. Because trends were calculated for each month of the year, data were purposefully not de-seasonalized prior to trend analysis. For PAR data and SST data, month-wise trends over time were calculated using Theil-Sen non-parametric estimates of slope over time at each x,y location, and the significance of those trends was assessed using Mann-Kendall tests. To determine the significance of decadal differences in the daily time series of PAR and SST, we applied Kruskal-Wallis tests to compare each day-of-year mean for 2001-2011 to the same day-of-year mean for 2012-2022 for each ecoregion. Since we analyzed the seasonal pattern for each decade, we purposefully did not de-seasonalize the data prior to decadal comparisons.

3. RESULTS

3.1. Patterns in seasonal Chl-a timing

Monthly patterns in Chl-a show an overall offshore-to-onshore shift in the location of high Chl-a from September to February (Fig. 2). Offshore, the months of October to December show the highest Chl-a, while over the shelf and coast, January to March experience the highest Chl-a. During the summer and fall (January to April) there is a strong north-to-south gradient of increasing Chl-a with latitude. The highest Chl-a concentrations occur in the southern shelf during the summer months of January and February (Fig. 2).

Phenology metrics, including long-term mean start date and peak date, varied with latitude and distance from shore (Fig. 3, Table 1). The long-term mean timing of the start of the accumulation season showed a smooth spatial pattern from offshore to onshore and from north to south, with start dates for the SPF, MIZ, northern shelf, mid shelf, and southern shelf occurring in September, October, November, December, and January, respectively (Fig. 3a, Table 1). For

peak date, the long-term mean was characterized by similar spatial patterns, although peak dates lagged start dates by approximately one to two months. Peak dates ranged from early December in the offshore SPF to mid-February over the southern shelf (Fig. 3b, Table 1).

Decadal seasonal cycles of daily Chl-a shifted later in the season for most ecoregions (Fig. 4, Table 2). In the MIZ, the phytoplankton accumulation season started later and ended earlier in 2012-2022 compared to 2001-2011, shortening the length of the accumulation season (Fig. 4b). The mid shelf experienced the largest shift toward later seasonal timing, with a start date becoming later by 19 days from one decade to the next (Fig. 4d). The northern shelf and southern shelf ecoregions showed slightly later timing of Chl-a, with start dates up to two weeks later in 2012-2022 than in 2001-2011. In the fall season, the strongest shifts toward higher fall Chl-a occurred in the SPF (Fig. 4a) and the northern shelf (Fig. 4c).

Spatially, from 2001-2011 to 2012-2022, the start date of the phytoplankton accumulation season became later along the shelf break and slope (Fig. 5), with decadal differences of to up to 30 days later over parts of the shelf, just offshore of the shelf break, and in most of the MIZ (Fig. 5c). In the far offshore environment, start dates shifted slightly earlier in recent years compared to past years (Fig. 5c). Peak date by decade also shifted later in the season (Fig. 5), with decadal differences of up to 40 days later in 2012-2022 compared to 2001-2011 (Fig. 5c). The shift to later peak dates was spatially most remarkable along and just offshore of the continental shelf break (Fig. 5d, 5e, 5f).

In terms of decadal differences by ecoregion, both start dates and peak dates shifted later in some ecoregions, yet other shifts were not statistically significant (Table 2, Fig. 6, Fig. 7). Start dates were significantly later in recent years compared to past years in the MIZ (Kruskal-Wallis test; chi square = 5.85, $p = 0.016$, df = 1), the northern shelf (chi square = 6.61, $p = 0.010$,

df = 1), and the mid shelf (chi square = 6.22, p = 0.013, df = 1) by 10 to 19 days (Table 2, Fig 6). Peak dates were significantly later in 2012-2022 compared to 2001-2011 in the MIZ (chi square = 8.69, p = 0.003, df = 1) and the northern shelf (chi square = 4.48, p = 0.034, df = 1) by 16 and 29 days, respectively (Table 2, Fig. 7). In terms of long-term trends by ecoregion, peak date showed the strongest trends toward later timing in the SPF and MIZ (Table 3), becoming 1 day later per year in the SPF (Theil-Sen slope; Mann-Kendall significance test; p = 0.007) and 1.5 days later per year in the MIZ (p = 0.018).

In terms of mapped long-term trends, the start date of the accumulation season shifted later over time over most of the continental shelf and most of the areas south of 64°S latitude, with varying levels of statistical significance (Fig. 8). For the offshore environment (west of 69°W and north of 63°S), there were isolated patches where start dates became earlier over time (Fig. 8a). However, much of the WAP region showed start dates getting later over time (i.e., 49% of the study area; Fig. 8a). Areas with strong trends toward later start date included the northern coast of the South Shetland Islands, over the continental shelf and coast just north and west of Adelaide Island, and farther offshore over the continental slope and deeper waters (south of 64°S and west of 70°W; Fig. 8a). Peak dates generally shifted later in the season over time, with an especially strong trend in the MIZ just offshore of the continental shelf break and slope north of 63°S latitude (Fig. 8b).

3.2. Overall satellite-derived Chl-a magnitude trends

Long-term trends from 1997 to 2022 in Chl-a concentration were on the order of +/- 0.01% yr^{-1} with high annual and interannual variability (Fig. S12 in the Supplement), unless resolved on monthly timescales (Fig. 9). By ecoregion, trends over time were minimal with the exception of the SPF (Table 4). Chl-a increased significantly over time in the SPF (Theil-Sen

379 slope; Mann-Kendall significance test; 0.03 % yr^{-1}; p = 0.004) from 1997 to 2022 (Table 4). All
380 other ecoregions showed minimal Chl-a trends over time (up to +/- 0.02 % yr^{-1} at most) with no
381 statistical significance (p > 0.198) (Table 4).

382 On monthly timescales, long-term Chl-a trends over time were larger in magnitude,
383 decreasing over time in spring (October to November) and increasing over time in summer and
384 fall (January to April) (Fig. 9). October and November showed evidence of strongly decreasing
385 Chl-a in the offshore to outer continental shelf regions, reaching -4 and -5 % yr^{-1}, respectively
386 (Fig. 9b,c). January, February, March, and April all showed slight increasing trends in Chl-a on
387 the order of 1 to 4 % yr^{-1} (Fig. 9e-h). In summer and fall, statistically significant increases were
388 located mostly offshore of the continental shelf. Nearshore waters showed more variability in the
389 direction of the trends from January through April.

390 **3.3. Trends in environmental variables**

391 Wind speed trends 1997 to 2022 in individual months show different long-term trends in
392 separate parts of the seasonal cycle. Wind speed is increasing over time most notably for the
393 month of November (Fig. 10). Spring months September, October, and November show
394 increasing wind speed over time. Summer months December and January show slight decreasing
395 trends in wind speed. Fall months display mixed trends, with February and March experiencing
396 increasing wind speed over time while April shows decreasing wind speed over time (Fig. 10).
397 While there is an overall increase in wind speed from 2001-2011 to 2012-2022, especially in the
398 offshore environment, wind direction does not show a substantial change and remains
399 predominantly northwesterly throughout the time series (Fig. S13 in the Supplement).

400 Analysis of PAR and SST data 1997 to 2022 did not reveal meaningful trends. We found
401 that the seasonal patterns in PAR were not significantly different between decades for any

ecoregion (Fig. S14 in the Supplement). By month, trends in PAR showed slight decreases over time (Fig. S15 in the Supplement), yet the seasonality of the PAR decreases did not correspond with the seasonality of the Chl-a trends observed (Fig. 9). Likewise, no significant difference was seen in the seasonal cycle of SST between decades (Fig. S16 in the Supplement). By month, SST trends show Septembers becoming slightly warmer, with no other significant trends in any other month in any ecoregion (Fig. S17 in the Supplement).

4. DISCUSSION

4.1. Assessing seasonality of phytoplankton

Although the "spring bloom" has been characterized for nearly one hundred years (Gran & Braarud 1935), studies of phytoplankton phenology in the global ocean differ on the most representative definition of the start date according to different metrics of bloom initiation. Most biomass-based estimates customarily point to the spring season as the start of the phytoplankton accumulation season rather than winter, varying depending on nutrient availability, latitude, and climatological factors. Often, start date co-occurs with the physical stratification of the water column (Sverdrup 1953, Siegel et al. 2002). Some argue that the seasonal cycle of phytoplankton growth truly begins in winter when conditions are well-mixed, according to the dilution hypothesis (Behrenfeld & Boss 2014). Due to limited information about loss rates (i.e., grazing, viruses, sinking) over the time and space scales needed for this analysis, in this paper we focus on phytoplankton accumulation, the seasonal period of increasing phytoplankton biomass (as measured by surface Chl-a concentration) when the average phytoplankton mass-specific loss rates are smaller than growth rates (Evans & Parslow 1985, Banse 1992, Behrenfeld & Boss 2018, Arteaga et al. 2020). Many studies also calculate the timing of the phytoplankton accumulation season start date based on biomass increase, such as the date when Chl-a rises

above a pre-defined threshold value (Siegel et al. 2002, Racault et al. 2012). Other approaches use the timing of the peak in the daily rate of change, the date when the cumulative sum of Chl-a rises above a certain value, and the date of the largest step change in the cumulative sum of anomalies in Chl-a (Brody et al. 2013, Thomalla et al. 2015). Through a sensitivity analysis evaluating a variety of published metrics, we demonstrate that our methods and conclusions applying the threshold metric are robust (Fig. S10 in the Supplement).

4.2. Decadal shifts in bloom phenology

Phytoplankton accumulation season start dates and peak dates are shifting later in the season, and Chl-a is remaining higher for longer into the fall season (Fig. 4, 5, 9). Start date is occurring later over time especially in the MIZ and over the shelf (Fig. 4b, 5c, 6) and peak date is becoming later over time especially just offshore of the shelf break (Fig. 5f, 7, 8). Decadal differences may be muted slightly (Fig. 6, 7) when averaged over space and time, as the averaging likely masks the strong trends seen along the continental shelf break in the MIZ (Fig. 5). Chl-a trends by month further support the shift toward later timing each season, as October and November show long-term decreases in Chl-a, while January to April show long-term increases in Chl-a (Fig. 9). Although global climate models predict earlier spring blooms in polar regions, in the WAP region we saw a shift toward later spring start dates and later summer peak dates over time.

While the timing of the phytoplankton accumulation season is generally shifting later, by ecoregion, phenology is trending in mixed directions. Our results reveal that offshore open ocean spring blooms are shifting earlier while blooms in ice-associated ecoregions shift later. These results are not mutually exclusive and can both be simultaneously occurring. The open ocean environment of the SPF is very different from the MIZ and shelf, since the latter environments

448 experience sea ice coverage for a substantial portion of the year. The different level of exposure
449 to sea ice may contribute to the different trends in phytoplankton phenology for the open ocean
450 environment compared to the ice-influenced ecoregions. These diverging trends represent a
451 temporal widening in the bloom timing between the open ocean environment and the ice-
452 influenced environment. If this divergence continues in future years, ecological consequences
453 could further differentiate these two systems as the effects of the shifting bloom timing propagate
454 throughout the marine food web.

455 **4.3. Potential mechanisms for seasonal shifts**

456 Possible drivers behind observed seasonal shifts in timing include changes in wind speed,
457 cloud cover, temperature, and sea ice dynamics. Wind speed is the most likely mechanism for
458 change in spring start dates (Fig. 10). A long-term increase in wind mixing has likely decreased
459 early season water column stability, suppressing phytoplankton accumulation (Fig. 11). Other
460 available environmental data (i.e., PAR, SST) cannot explain the patterns observed in shifting
461 Chl-a phenology.

462 4.3.1. Increased spring wind speed

463 Wind speed trends 1997-2022 in individual months support the idea that enhanced winds
464 could suppress an early spring bloom in the WAP. Wind speed is increasing over time for the
465 month of November (Fig. 10), concurrent with October and November showing later
466 phytoplankton accumulation season start dates (Fig. 9). Our observations of increasing wind
467 speed are consistent with other findings that spring (September-November) wind speed is
468 increasing over time for the broader West Antarctica sector of the Southern Ocean (Yu et al.
469 2020). Due to increased spring wind speeds in recent years, seasonal water column stratification
470 from sea ice melt may not be occurring early enough to support an early spring bloom. Although

471 there is evidence of a shallowing summer mixed layer depth over time based on the month of
472 January (Brown et al. 2019), it is nevertheless possible that the onset of the spring MLD
473 shallowing is now happening later in the season each year. For the WAP, as the system
474 progresses toward lower sea ice extent and shorter sea ice duration, wind mixing may be possible
475 throughout more of each year in a low-ice state. A similar relationship between ice retreat, high
476 wind speeds, and later bloom initiation was seen in the Bering Sea, a polar system experiencing
477 long-term declines in seasonal sea ice. In years with early sea ice retreat (Boreal early spring,
478 before mid-March), the spring phytoplankton bloom was delayed until the water columns
479 stratified with warming air temperatures and increased sunlight (Stabeno et al. 2001, 2012).
480 We developed a conceptual diagram for the difference between past conditions and recent
481 conditions in the MIZ in spring to contextualize our results (Fig. 11). In spring, in the MIZ, the
482 past had more sea ice and lower wind speeds, resulting in a shallower mixed layer depth. Light-
483 limitation depth in this conceptual diagram is illustrated as a range of depths falling between
484 Sverdrup's (1953) shallower critical depth definition with a liberal compensation irradiance and
485 a more conservative deeper light-limitation depth corresponding to a smaller compensation
486 irradiance (Geider et al. 1986, Behrenfeld & Boss 2018). With increased wind speeds under
487 present conditions, mixed layer depth deepens. Increased spring wind speeds over time are
488 especially prevalent in the month of November (Fig. 10). However, we found no long-term
489 change in PAR (Fig. S14, S15 in the Supplement). Spring conditions are inherently light limited
490 due to low solar zenith angles (SZA) at these high latitudes. At the same spring light levels, with
491 the MLD deepening due to higher wind speeds and less water column stability, phytoplankton
492 are likely more light-limited under present conditions compared to the past.
493 4.3.2. Other environmental data fail to explain seasonal Chl-a shifts

Other potential mechanisms for later start dates include 1) a reduction in PAR due to increased cloud cover or 2) a shift in SST. Previous studies have shown evidence of a long-term increase in cloud cover and precipitation over the WAP (Kirchgäßner 2009, 2011, Datta et al. 2019, Sato & Simmonds 2021). Cloudier conditions with lower PAR would further limit an earlier start to the phytoplankton accumulation season if combined with enhanced wind mixing. Temperature acts as a major control on phytoplankton phenology in the global ocean, including the growth preference for different species and the length of the phytoplankton accumulation season in different ocean biomes (Racault et al. 2012, Poloczanska et al. 2016, Leeuwe et al. 2020). Shifts in SST could therefore theoretically alter the start date and peak date of the accumulation season. However, according to our analysis, long-term change in the seasonal timing of PAR (Fig. S14, S15 in the Supplement) and SST (Fig. S16, S17 in the Supplement) are not driving factors for the observed shifts in Chl-a phenology.

One final potential mechanism for later phytoplankton timing may be sea ice decline. A decrease in sea-ice-melt-induced water column stability would suppress spring phytoplankton accumulation. However, this sea ice explanation may be confounded by other factors. Venables et al. (2013) present evidence that the timing of bloom initiation in the WAP follows light availability rather than sea ice retreat, and that low- and high-ice years showed similar bloom initiation dates. Our results support this idea, as the progression toward later start dates is not clearly mirrored by a progression toward later sea ice retreat over the same set of corresponding years. (Fig. S18 in the Supplement). It is possible that the lack of correlation between spring Chl-a trends and sea ice trends is due to the potential that satellites now miss the earliest ice-edge bloom. In slope and offshore waters, the ice-edge bloom occurred later in the season in past decades. In recent years, if the ice-edge bloom is occurring in late winter or early spring before

satellites have sufficient sun angle to get reliable data, e.g., August (Fig. 2), satellites cannot capture the earliest bloom. In that case, our results indicate that the non-ice-edge bloom is beginning later over time (Fig. 4), implying that the later phytoplankton accumulation timing is not directly associated with changes in sea ice dynamics. Fluctuations in sea ice dynamics are linked to oscillations of the Southern Annular Mode (SAM) and changes in wind speed and direction (Stammerjohn et al. 2003, 2008, Turner et al. 2013). Our results show increasing wind speed over the offshore waters from the northwest, consistent with a long-term trend toward a positive SAM, without a concurrent change in wind direction (Fig. S13). As the region experiences future shifts in sea ice extent and duration, future interactions between the SAM, wind speed, sea ice, and phytoplankton merit further study.

4.4. Ecological impacts of shifting phenology

Phytoplankton represent the base of this dynamic food web, thus shifts in phytoplankton seasonal timing may impact the feeding, migration, and breeding behaviors of higher trophic level organisms. The MIZ provides critical habitat for krill, fishes, seabirds, pinnipeds, and cetaceans. While krill may have the ability to shift their phenology in response to interannual variability in environmental conditions (Conroy et al. 2023), the relative abundance of other species such as salps and pteropods can enhance grazing pressure on phytoplankton (Bernard et al. 2012). Zooplankton grazing can act as an important control on phytoplankton bloom duration as seen in other parts of coastal Antarctica (Kauko et al. 2021), thus effects of changes in grazing on phytoplankton phenology in the WAP region merit further study. Changing phenology at the base of the food web could additionally disrupt the life history strategies of keystone species such as Antarctic Silverfish, Adélie penguins, and humpback whales (Fraser et al. 1992, Saba et

al. 2014, Weinstein & Friedlaender 2017, Henley et al. 2019, Cimino et al. 2019, 2023, Corso et al. 2022).

The results of the present study suggest that start dates and peak dates of the phytoplankton accumulation season are occurring later in the marginal ice zone and fall phytoplankton biomass is persisting later in the season over time over the northern continental shelf. Spring shifts and fall shifts may have different ecological implications. In spring, overall the WAP ecosystem is less "predictable" during years with earlier spring sea ice retreat when the timing of phenological events throughout the food web is more diverse (i.e., higher variability in timing) (Cimino et al. 2023). This implies that as the system shifts experiences further sea ice decline in future years, the timing of events in spring may become increasingly variable. In fall, higher Chl-a concentrations in recent years (Fig. 4, 9) could provide a sustained food source for zooplankton and higher trophic levels later into the season than in past years. This shift toward a highly productive fall season in recent years could have implications for higher trophic level organism life history strategies.

4.5. Impact on annual carbon uptake

Results imply that annual biological carbon uptake may not be changing substantially over time 1997-2022, because both spring and fall processes are shifting later in the season and the overall trend in Chl-a is minimal. While the timing of events each season is shifting later in the season over time, the total magnitude of Chl-a is only minimally changing over time (Fig. S9 in the Supplement). In the middle of the austral summer, the generally increasing Chl-a trend observed in January in the present study (Fig. 9e) corresponds with the results of Brown et al. (2019) showing increasing in situ Chl-a based on data collected during summer months. Furthermore, the statistically significant Chl-a increases in the SPF (Table 4) align with the

overall "greening" of the Southern Ocean observed by Del Castillo et al. (2019) and Pinkerton et al. (2021). This offshore environment is quite different from the coastal WAP ecoregions in that it is typically defined as a High Nutrient Low Chlorophyll ecosystem and is considered to be an oligotrophic area (Tréguer & Jacques 1992), with long-term mean Chl-a concentrations ≤ 0.4 mg m^{-3} (Fig. S12 in the Supplement). The results of the present study show smaller-magnitude Chl-a trends than those presented by Montes-Hugo et al. (2009), which likely had significant biases using the older CZCS data (Fig. S1, S2 in the Supplement). Generally, small-magnitude changes in Chl-a suggest that despite the warming temperatures and generally lower sea ice conditions compared to the past, the WAP is not experiencing long-term declines in phytoplankton biomass.

Changes in the timing of the phytoplankton accumulation season may affect the timing and magnitude of biological CO_2 uptake. Biological production drives variability in air-sea CO_2 exchange along the WAP (Carrillo et al. 2004, Eveleth et al. 2017). Since the mid-2000s, several studies utilizing pCO_2 observations suggest a strengthening of Southern Ocean CO_2 uptake (Xue et al. 2015, Landschützer et al. 2015, Munro et al. 2015b). However, the seasonal timing of when this strengthening is occurring is still unknown. Our results suggest austral fall may be experiencing higher Chl-a concentration than in the past (Fig. 4, 9), possibly strengthening CO_2 uptake in the fall months. Overall, the amplitude of the seasonal cycle in surface pCO_2 is small, because the thermal and biological components of the seasonal cycle balance one another (Munro et al. 2015a). This suggests that at the seasonal scale, impacts of warm summer temperatures on carbon uptake are balanced by biological CO_2 uptake. Phytoplankton phenology shifts show later spring start dates and higher fall Chl-a, but this shift is seen in the timing of the biological carbon uptake rather than the magnitude. The connection between Chl-a and carbon cycling depends on many factors other than the magnitude of the bloom or its timing (Henley et

al. 2020). For example, Chl-a often increases before phytoplankton carbon in the Southern Ocean spring bloom (Vives et al. 2023). Whether there has been a change in the total annual carbon uptake based on changing Chl-a timing remains to be seen and merits further study. Our results imply that phytoplankton biomass is not changing in the long term despite phenological shifts toward later start date in spring and higher Chl-a in fall.

4.6. Future outlook

Changing Chl-a phenology may relate to changing phytoplankton community composition. Although data from Palmer Station (in the mid shelf ecoregion in this study) shows diatoms as the first species to bloom (Nardelli et al. 2023), other studies find that the haptophyte *Phaeocystis antarctica* is the dominant first bloomer, not diatoms, especially in offshore waters from the continental shelf break outwards (Arrigo et al. 2017, Joy-Warren et al. 2019). Because the strongest shifts in the timing of start date and peak date are occurring along the continental shelf break in our results (Fig. 5), it is possible that these changes are affecting haptophytes, but more work is needed to discern phytoplankton species with temporal coverage over the entire season. Future work will explore algorithms to leverage upcoming hyperspectral satellite missions (Dierssen et al. 2021) to remotely detect different phytoplankton groups going forward in this dynamic and rapidly changing region of the Southern Ocean.

Continued long-term in situ monitoring is critical to maintain in this region to further validate remote sensing algorithms and explore potential new technologies for assessing biodiversity and biogeochemistry. High solar zenith angle at high latitudes in the Southern hemisphere limit temporal coverage of passive ocean color measurements, making winter months May to August unretrievable (Fig. 2 and Fig. S7 in the Supplement) and early spring and late fall retrievals (September, April) more prone to error due to the longer pathlength through

608 Earth's atmosphere. Additionally, satellite-derived Chl-a estimates only apply during cloud-free
609 conditions and only in the surface ocean. Studies show that Chl-a maximum concentrations often
610 occur at depths as deep as 75 to 100 m that cannot be assessed directly with passive ocean color
611 measurements (Holm-Hansen & Hewes 2004). These biases can be mitigated in future work
612 using data from profiling biogeochemical-Argo floats (e.g., Arteaga et al. 2020, Hague & Vichi
613 2021) and airborne and space-based lidar to better understand what happens in Antarctic waters
614 at times and depths for which satellite observations are not available. Space-based lidar has the
615 potential to estimate phytoplankton biomass within the first three optical depths for more
616 representative phytoplankton physiology measurements from space (Behrenfeld et al. 2017).
617 Thus, merging field data and advanced modeling (Kim et al. 2021) with new technology, such as
618 hyperspectral drones (Joyce et al. 2019) and airborne and space-based lidar (Behrenfeld et al.
619 2017, Bisson et al. 2021) will allow us to better explore changes in this dynamic region. Future
620 work will also be improved by the increasing length of the time series. Although 25 years of
621 ocean color data represent a valuable resource, the time series is still relatively short. Modeling
622 studies have revealed that at high latitudes, 20 to 40 years of data are needed to illuminate
623 climate relevant trends in ocean primary production (Henson et al., 2013; 2018). With the launch
624 of the next generation of hyperspectral satellite missions like NASA's Plankton, Aerosols,
625 Clouds, and ocean Ecosystems (PACE) and Surface Biology and Geology (SBG) over the next
626 decade (Dierssen et al. 2023), we will continue to investigate these long-term bloom phenology
627 trends and impacts on the trophic web in this dynamic polar ecosystem.
628
629 ***Acknowledgments:*** Funding for this work was provided by NASA Interdisciplinary Science
630 (IDS) award number 80NSSC20K1518 and NSF Office of Polar Programs Postdoctoral

631 Fellowship to J. Turner award number 2317774. Additional funding comes from Palmer Long
632 Term Ecological Research grant NSF LTER-2026045. Ocean color data used in satellite-derived
633 Chl-a analysis are available from CMEMS at
634 https://data.marine.copernicus.eu/product/OCEANCOLOUR_GLO_BGC_L4_MY_009_104/ser
635 vices (Dataset: Cmems_obs-oc_glo_bgc-plankton_my_l4-gapfree-multi-4km_p1d). Wind data
636 are available from ECMWF via the Copernicus Climate Data Store at
637 https://cds.climate.copernicus.eu/cdsapp#!/dataset/reanalysis-era5-single-levels?tab=form
638 (Dataset: ERA5 hourly data on single levels from 1940 to present). PAR data are available from
639 NASA ocean color web at https://oceancolor.gsfc.nasa.gov/ (Dataset: Photosynthetically
640 Available Radiation (PAR)). SST data are available from CMEMS at
641 https://data.marine.copernicus.eu/product/SST_GLO_SST_L4_REP_OBSERVATIONS_010_01
642 1/services (Dataset: METOFFICE-GLO-SST-L4-REP-OBS-SST). Code used to make figures is
643 available at https://doi.xxxx (doi forthcoming, files available at temporary link:
644 https://app.box.com/s/c00pvlet5z90bwhavera1czqgfywiusf). Mapping help was provided by
645 Schuyler Nardelli and Jack Conroy. We thank Emmanuel Boss and two anonymous reviewers
646 for their helpful comments during the peer review process. The authors declare no conflicts of
647 interest.

LITERATURE CITED

Arrigo KR, van Dijken G, Long M (2008) Coastal Southern Ocean: A strong anthropogenic CO_2 sink. Geophys Res Lett 35:1–6.

Arrigo KR, van Dijken GL, Alderkamp AC, Erickson ZK, Lewis KM, Lowry KE, Joy-Warren HL, Middag R, Nash-Arrigo JE, Selz V, van de Poll W (2017) Early spring phytoplankton dynamics in the western Antarctic Peninsula. J Geophys Res Oceans 122:9350–9369.

Arrigo KR, McClain CR (1994) Spring phytoplankton production in the western Ross Sea. Science 266:261–263.

Arteaga LA, Boss E, Behrenfeld MJ, Westberry TK, Sarmiento JL (2020) Seasonal modulation of phytoplankton biomass in the Southern Ocean. Nat Commun 11:5364.

Babin M, Morel A, Gentili B (1996) Remote sensing of sea surface Sun-induced chlorophyll fluorescence: consequences of natural variations in the optical characteristics of phytoplankton and the quantum yield of chlorophyll a fluorescence. Int J Remote Sens 17:2417–2448.

Banse K (1992) Grazing, temporal changes of phytoplankton concentrations, and the microbial loop in the open sea. In: *Primary Productivity and Biogeochemical Cycles in the Sea*. Springer, Boston, MA, p 409–440

Barbieux M, Uitz J, Bricaud A, Organelli E, Poteau A, Schmechtig C, Gentili B, Obolensky G, Leymarie E, Penkerc'h C, D'Ortenzio F, Claustre H (2018) Assessing the variability in the relationship between the particulate backscattering coefficient and the Chlorophyll *a* concentration from a global Biogeochemical-Argo database. J Geophys Res Oceans 123:1229–1250.

Behrenfeld MJ, Boss ES (2014) Resurrecting the ecological underpinnings of ocean plankton blooms. Annu Rev Mar Sci 6:167–194.

Behrenfeld MJ, Boss ES (2018) Student's tutorial on bloom hypotheses in the context of phytoplankton annual cycles. Glob Change Biol 24:55–77.

Behrenfeld MJ, Hu Y, O'Malley RT, Boss ES, Hostetler CA, Siegel DA, Sarmiento JL, Schulien J, Hair JW, Lu X, Rodier S, Scarino AJ (2017) Annual boom-bust cycles of polar phytoplankton biomass revealed by space-based lidar. Nat Geosci 10:118–122.

Bernard KS, Steinberg DK, Schofield OME (2012) Summertime grazing impact of the dominant macrozooplankton off the Western Antarctic Peninsula. Deep Sea Res Part Oceanogr Res Pap 62:111–122.

Bisson KM, Boss E, Werdell PJ, Ibrahim A, Behrenfeld MJ (2021) Particulate backscattering in the global ocean: A comparison of independent assessments. Geophys Res Lett 48:e2020GL090909.

Boss E, Behrenfeld M (2010) In situ evaluation of the initiation of the North Atlantic phytoplankton bloom. Geophys Res Lett 37:L18603.

Brody SR, Lozier MS, Dunne JP (2013) A comparison of methods to determine phytoplankton bloom initiation. J Geophys Res Oceans 118:2345–2357.

Brown MS, Munro DR, Feehan CJ, Sweeney C, Ducklow HW, Schofield OM (2019) Enhanced oceanic CO_2 uptake along the rapidly changing West Antarctic Peninsula. Nat Clim Change 9:678–683.

C3S (2018) ERA5: Fifth generation of ECMWF atmospheric reanalyses of the global climate. Copernicus Climate Change Service. https://cds.climate.copernicus.eu/cdsapp#!/home (accessed April 25, 2022)

Carrillo CJ, Smith RC, Karl DM (2004) Processes regulating oxygen and carbon dioxide in surface waters west of the Antarctic Peninsula. Mar Chem 84:161–179.

Carvalho F, Kohut J, Oliver MJ, Sherrell RM, Schofield O (2015) Mixing and phytoplankton dynamics in a submarine canyon in the West Antarctic Peninsula. J Geophys Res Oceans 121:5069–5083.

Chapman CC, Lea M-A, Meyer A, Sallée J-B, Hindell M (2020) Defining Southern Ocean fronts and their influence on biological and physical processes in a changing climate. Nat Clim Change 10:209–219.

Cimino MA, Conroy JA, Connors E, Bowman J, Corso A, Ducklow H, Fraser W, Friedlaender A, Kim HH, Larsen GD, Moffat C, Nichols R, Pallin L, Patterson-Fraser D, Roberts D, Roberts M, Steinberg DK, Thibodeau P, Trinh R, Schofield O, Stammerjohn S (2023) Long-term patterns in ecosystem phenology near Palmer Station, Antarctica, from the perspective of the Adélie penguin. Ecosphere 14.

Cimino MA, Patterson-Fraser DL, Stammerjohn S, Fraser WR (2019) The interaction between island geomorphology and environmental parameters drives Adélie penguin breeding phenology on neighboring islands near Palmer Station, Antarctica. Ecol Evol 9:9334–9349.

Cleveland JS, Perry MJ, Kiefer DA, Talbot MC (1989) Maximal quantum yield of photosynthesis in the northwestern Sargasso Sea. J Mar Res 47:869–886.

Conroy J, Steinberg D, Thomas M, West L (2023) Seasonal and interannual changes in a coastal Antarctic zooplankton community. Mar Ecol Prog Ser 706:17–32.

Corso AD, Steinberg DK, Stammerjohn SE, Hilton EJ (2022) Climate drives long-term change in Antarctic Silverfish along the western Antarctic Peninsula. Commun Biol 5:1–10.

Danziger Z (2024) Theil-Sen Robust Linear Regression.

Datta RT, Tedesco M, Fettweis X, Agosta C, Lhermitte S, Lenaerts JTM, Wever N (2019) The effect of foehn-induced surface melt on firn evolution over the Northeast Antarctic Peninsula. Geophys Res Lett 46:3822–3831.

Del Castillo CE, Signorini SR, Karaköylü EM, Rivero-Calle S (2019) Is the Southern Ocean getting greener? Geophys Res Lett 46:6034–6040.

Dierssen HM (2000) Ocean color remote sensing of chlorophyll and primary production west of the Antarctic Peninsula. Ph.D. Dissertation. University of California Santa Barbara.

Dierssen HM, Ackleson SG, Joyce KE, Hestir EL, Castagna A, Lavender S, McManus MA (2021) Living up to the hype of hyperspectral aquatic remote sensing: science, resources and outlook. Front Environ Sci 9:649528.

Dierssen HM, Gierach M, Guild LS, Mannino A, Salisbury J, Schollaert Uz S, Scott J, Townsend PA, Turpie K, Tzortziou M, Urquhart E, Vandermeulen R, Werdell PJ (2023) Synergies between NASA's hyperspectral aquatic missions PACE, GLIMR, and SBG: Opportunities for new science and applications. J Geophys Res Biogeosciences 128:e2023JG007574.

Dierssen HM, Smith RC (2000) Bio-optical properties and remote sensing ocean color algorithms for Antarctic Peninsula waters. J Geophys Res 105:26301–26312.

Dierssen HM, Smith RC, Vernet M (2002) Glacial meltwater dynamics in coastal waters west of the Antarctic peninsula. Proc Natl Acad Sci U S A 99:1790–1795.

738 Dierssen HM, Vernet M, Smith RC (2000) Optimizing models for remotely estimating primary
739 production in Antarctic coastal waters. Antarct Sci 12:20–32.
740 Evans GT, Parslow JS (1985) A model of annual plankton cycles. Biol Oceanogr 3:327–347.
741 Eveleth R, Cassar N, Doney SC, Munro DR, Sweeney C (2017) Biological and physical controls
742 on O_2/Ar, Ar and pCO_2 variability at the Western Antarctic Peninsula and in the Drake
743 Passage. Deep Sea Res Part II Top Stud Oceanogr 139:77–88.
744 Fenchel T (1988) Marine plankton food chains. Annu Rev Ecol Syst 19:19–38.
745 Fraser WR, Trivelpiece WZ, Ainley DG, Trivelpiece SG (1992) Increases in Antarctic penguin
746 populations: reduced competition with whales or a loss of sea ice due to environmental
747 warming? Polar Biol 11.
748 Friedland KD, Mouw CB, Asch RG, Ferreira ASA, Henson S, Hyde KJW, Morse RE, Thomas
749 AC, Brady DC (2018) Phenology and time series trends of the dominant seasonal
750 phytoplankton bloom across global scales. Glob Ecol Biogeogr 27:551–569.
751 Frouin R, Franz BA, Werdell PJ (2002) The SeaWiFS PAR product. ,In: S.B. Hooker and E.R.
752 Firestone, Algorithm Updates for the Fourth SeaWiFS Data Reprocessing, NASA Tech.
753 Memo. 2003-206892, Volume 22, NASA Goddard Space Flight Center, Greenbelt,
754 Maryland, 46-50.
755 Frouin R, McPherson J, Ueyoshi K, Franz BA (2012) A time series of photosynthetically
756 available radiation at the ocean surface from SeaWiFS and MODIS data.Frouin R,
757 Ebuchi N, Pan D, Saino T (eds) Kyoto, Japan
758 Frouin R, Pinker RT (1995) Estimating Photosynthetically Active Radiation (PAR) at the Earth's
759 surface from satellite observations. Remote Sens Environ 51:98–107.
760 Garnesson P, Mangin A, D'Andon OF, Demaria J, Bretagnon M (2019) The CMEMS
761 GlobColour chlorophyll a product based on satellite observation: Multi-sensor merging
762 and flagging strategies. Ocean Sci 15:819–830.
763 Geider RJ, MacIntyre H, Kana T (1997) Dynamic model of phytoplankton growth and
764 acclimation:responses of the balanced growth rate and the chlorophyll a:carbon ratio to
765 light, nutrient-limitation and temperature. Mar Ecol Prog Ser 148:187–200.
766 Geider RJ, Osbonie BA, Raven JA (1986) Growth, photosynthesis, and maintenance metabolic
767 cost in the diatom *Phaeodactylum tricornutum* at very low light levels. J Phycol 22:39–
768 48.
769 Gilbert RO (1987) 6.5 Sen's Nonparametric Estimator of Slope. In: *Statistical methods for*
770 *environmental pollution monitoring*. John Wiley & Sons, Hoboken, NJ
771 Gohin F, Druon JN, Lampert L (2002) A five channel chlorophyll concentration algorithm
772 applied to SeaWiFS data processed by SeaDAS in coastal waters. Int J Remote Sens
773 23:1639–1661.
774 Good S, Fiedler E, Mao C, Martin MJ, Maycock A, Reid R, Roberts-Jones J, Searle T, Waters J,
775 While J, Worsfold M (2020) The current configuration of the OSTIA system for
776 operational production of foundation sea surface temperature and ice concentration
777 analyses. Remote Sens 12:720.
778 Gran HH, Braarud T (1935) A quantitative study of the phytoplankton in the Bay of Fundy and
779 the Gulf of Maine (including observations on hydrography, chemistry, and turbidity).
780 Biol Board Can 1:279–467.
781 Greene CA, Thirumalai K, Kearney KA, Delgado JM, Schwanghart W, Wolfenbarger NS,
782 Thyng KM, Gwyther DE, Gardner AS, Blankenship DD (2019) The Climate Data
783 Toolbox for MATLAB. Geochem Geophys Geosystems 20:3774–3781.

784 Haëntjens N, Boss E, Talley LD (2017) Revisiting ocean color algorithms for chlorophyll a and
785 particulate organic carbon in the Southern Ocean using biogeochemical floats. J Geophys
786 Res Oceans 122:6583–6593.
787 Hague M, Vichi M (2021) Southern Ocean Biogeochemical Argo detect under-ice phytoplankton
788 growth before sea ice retreat. Biogeosciences 18:25–38.
789 Henley SF, Cavan EL, Fawcett SE, Kerr R, Monteiro T, Sherrell RM, Bowie AR, Boyd PW,
790 Barnes DKA, Schloss IR, Marshall T, Flynn R, Smith S (2020) Changing
791 biogeochemistry of the Southern Ocean and its ecosystem implications. Front Mar Sci
792 7:581.
793 Henley SF, Schofield OM, Hendry KR, Schloss IR, Steinberg DK, Moffat C, Peck LS, Costa
794 DP, Bakker DCE, Hughes C, Rozema PD, Ducklow HW, Abele D, Stefels J, Van
795 Leeuwe MA, Brussaard CPD, Buma AGJ, Kohut J, Sahade R, Friedlaender AS,
796 Stammerjohn SE, Venables HJ, Meredith MP (2019) Variability and change in the west
797 Antarctic Peninsula marine system: Research priorities and opportunities. Prog Oceanogr
798 173:208–237.
799 Henson SA, Cole HS, Hopkins J, Martin AP, Yool A (2018) Detection of climate change-driven
800 trends in phytoplankton phenology. Glob Change Biol 24:e101–e111.
801 Holm-Hansen O, Hewes CD (2004) Deep chlorophyll-a maxima (DCMs) in Antarctic waters: I.
802 Relationships between DCMs and the physical, chemical, and optical conditions in the
803 upper water column. Polar Biol 27:699–710.
804 Hu C, Lee Z, Franz B (2012) Chlorophyll a algorithms for oligotrophic oceans: A novel
805 approach based on three-band reflectance difference. J Geophys Res Oceans 117:1–25.
806 IOCCG (2015) Ocean Colour Remote Sensing in Polar Seas. IOCCG Report Series, No. 16,
807 International Ocean Colour Coordinating Group, Dartmouth, Canada. Babin M, Arrigo
808 K, Belanger S, Forget M-H (eds).
809 IPCC (2019) IPCC Special Report on the Ocean and Cryosphere in a Changing Climate.
810 International Panel on Climate Change. Pörtner H-O, Roberts DC, Masson-Delmotte V,
811 Zhai P, Tignor E, Poloczanska K, Mintenbeck K, Alegría A, Nicolai M, Okem A, Petzold
812 J, Rama B, Weyer NM (eds) Cambridge University Press, Cambridge, UK and New York
813 NY, USA.
814 Jeandel C, Ruiz-Pino D, Gjata E, Poisson A, Brunet C, Charriaud E, Dehairs F, Delille D, Fiala
815 M, Fravalo C, Carlos Miquel J, Park Y-H, Pondaven P, Quéguiner B, Razouls S, Shauer
816 B, Tréguer P (1998) KERFIX, a time-series station in the Southern Ocean: a presentation.
817 J Mar Syst 17:555–569.
818 Joyce KE, Duce S, Leahy SM, Leon J, Maier SW (2019) Principles and practice of acquiring
819 drone-based image data in marine environments. Mar Freshw Res 70:952.
820 Joy-Warren HL, van Dijken GL, Alderkamp AC, Leventer A, Lewis KM, Selz V, Lowry KE,
821 van de Poll W, Arrigo KR (2019) Light is the primary driver of early season
822 phytoplankton production along the western Antarctic Peninsula. J Geophys Res Oceans
823 124:7375–7399.
824 Kahru M, Mitchell BG (2010) Blending of ocean colour algorithms applied to the Southern
825 Ocean. Remote Sens Lett 1:119–124.
826 Kauko HM, Hattermann T, Ryan-Keogh T, Singh A, De Steur L, Fransson A, Chierici M,
827 Falkenhaug T, Hallfredsson EH, Bratbak G, Tsagaraki T, Berge T, Zhou Q, Moreau S
828 (2021) Phenology and environmental control of phytoplankton blooms in the Kong
829 Håkon VII Hav in the Southern Ocean. Front Mar Sci 8:623856.

Kendall MG (1975) Rank Correlation Methods. Griffin, London.
Killick R, Fearnhead P, Eckley IA (2012) Optimal detection of changepoints with a linear computational cost. J Am Stat Assoc 107:1590–1598.
Kim HH, Ducklow HW, Abele D, Barlett EMR, Buma AGJ, Meredith MP, Rozema PD, Schofield OM, Venables HJ, Schloss IR (2018) Inter-decadal variability of phytoplankton biomass along the coastal West Antarctic Peninsula. Philos Trans R Soc Math Phys Eng Sci 376.
Kim HH, Luo Y-W, Ducklow H, Schofield O, Steinberg D, Doney S (2021) WAP-1D-VAR v1.0: Development and Evaluation of a One-Dimensional Variational Data Assimilation Model for the Marine Ecosystem Along the West Antarctic Peninsula. Geosci Model Dev Discuss:1–44.
Kirchgäßner A (2009) An analysis of cloud observations from Vernadsky, Antarctica. Int J Climatol 30:1431–1439.
Kirchgäßner A (2011) An analysis of precipitation data from the Antarctic base Faraday/Vernadsky. Int J Climatol 31:404–414.
Landschützer P, Gruber N, Haumann FA, Rödenbeck C, Bakker DCE, van Heuven S, Hoppema M, Metzl N, Sweeney C, Takahashi T, Tilbrook B, Wanninkhof R (2015) The reinvigoration of the Southern Ocean carbon sink. Science 349:1221–1224.
Leeuwe MA, Webb AL, Venables HJ, Visser RJW, Meredith MP, Elzenga JTM, Stefels J (2020) Annual patterns in phytoplankton phenology in Antarctic coastal waters explained by environmental drivers. Limnol Oceanogr 65:1651–1668.
Mann HB (1945) Nonparametric Tests Against Trend. Econometrica 13:245.
Martinson DG (2012) Antarctic circumpolar current's role in the Antarctic ice system: An overview. Palaeogeogr Palaeoclimatol Palaeoecol 335–336:71–74.
Meredith MP, Stammerjohn SE, Ducklow HW, Leng MJ, Arrowsmith C, Brearley JA, Venables HJ, Barham M, van Wessem JM, Schofield O, Waite N (2021) Local- and large-scale drivers of variability in the coastal freshwater budget of the Western Antarctic Peninsula. J Geophys Res Oceans 126:1–22.
Meredith MP, Stammerjohn SE, Venables HJ, Ducklow HW, Martinson DG, Iannuzzi RA, Leng MJ, van Wessem JM, Reijmer CH, Barrand NE (2017) Changing distributions of sea ice melt and meteoric water west of the Antarctic Peninsula. Deep-Sea Res Part II Top Stud Oceanogr 139:40–57.
Mitchell BG (1992) Predictive bio-optical relationships for polar oceans and marginal ice zones. J Mar Syst 3:91–105.
Mitchell BG, Holm-Hansen O (1991) Bio-optical properties of Antarctic Peninsula waters: differentiation from temperate ocean models. Deep Sea Res Part Oceanogr Res Pap 38:1009–1028.
Moline MA (1998) Photoadaptive response during the development of a coastal Antarctic diatom bloom and relationship to water column stability. Limnol Oceanogr 43:146–153.
Montes-Hugo M, Doney SC, Ducklow HW, Fraser W, Martinson D, Stammerjohn SE, Schofield O (2009) Recent changes in phytoplankton communities associated with rapid regional climate change along the Western Antarctic Peninsula. Science 323:1470–1473.
Munro DR, Lovenduski NS, Stephens BB, Newberger T, Arrigo KR, Takahashi T, Quay PD, Sprintall J, Freeman NM, Sweeney C (2015a) Estimates of net community production in the Southern Ocean determined from time series observations (2002–2011) of nutrients,

dissolved inorganic carbon, and surface ocean pCO2 in Drake Passage. Deep Sea Res Part II Top Stud Oceanogr 114:49–63.

Munro DR, Lovenduski NS, Takahashi T, Stephens BB, Newberger T, Sweeney C (2015b) Recent evidence for a strengthening CO_2 sink in the Southern Ocean from carbonate system measurements in the Drake Passage (2002–2015). Geophys Res Lett 42:7623–7630.

Nardelli SC, Gray PC, Stammerjohn SE, Schofield O (2023) Characterizing coastal phytoplankton seasonal succession patterns on the West Antarctic Peninsula. Limnol Oceanogr:lno.12314.

Norman L, Thomas DN, Stedmon CA, Granskog MA, Papadimitriou S, Krapp RH, Meiners KM, Lannuzel D, Van Der Merwe P, Dieckmann GS (2011) The characteristics of dissolved organic matter (DOM) and chromophoric dissolved organic matter (CDOM) in Antarctic sea ice. Deep Sea Res Part II Top Stud Oceanogr 58:1075–1091.

Orsi AH, Whitworth T, Nowlin WD (1995) On the meridional extent and fronts of the Antarctic Circumpolar Current. Deep Sea Res Part Oceanogr Res Pap 42:641–673.

Pan BJ, Vernet M, Reynolds RA, Greg Mitchell B (2019) The optical and biological properties of glacial meltwater in an Antarctic fjord. PLoS ONE 14:1–30.

Patterson KW (2000) Contribution of chromophoric dissolved organic matter to attenuation of ultraviolet radiation in three contrasting coastal areas. University of California Santa Barbara

Pinkerton MH, Boyd PW, Deppeler S, Hayward A, Höfer J, Moreau S (2021) Evidence for the impact of climate change on primary producers in the Southern Ocean. Front Ecol Evol 9:592027.

Poloczanska ES, Brown CJ, Sydeman WJ, Kiessling W, Schoeman DS, Moore PJ, Brander K, Bruno JF, Buckley LB, Burrows MT, Duarte CM, Halpern BS, Holding J, Kappel CV, O'Connor MI, Pandolfi JM, Parmesan C, Schwing F, Thompson SA, Richardson AJ (2013) Global imprint of climate change on marine life. Nat Clim Change 3:919–925.

Poloczanska ES, Burrows MT, Brown CJ, García Molinos J, Halpern BS, Hoegh-Guldberg O, Kappel CV, Moore PJ, Richardson AJ, Schoeman DS, Sydeman WJ (2016) Responses of marine organisms to climate change across oceans. Front Mar Sci 3.

Racault M-F, Le Quéré C, Buitenhuis E, Sathyendranath S, Platt T (2012) Phytoplankton phenology in the global ocean. Ecol Indic 14:152–163.

Racault M-F, Raitsos DE, Berumen ML, Brewin RJW, Platt T, Sathyendranath S, Hoteit I (2015) Phytoplankton phenology indices in coral reef ecosystems: Application to ocean-color observations in the Red Sea. Remote Sens Environ 160:222–234.

Riley GA (1942) The relationship of vertical turbulence and spring diatom flowerings. J Mar Res 5:67–87.

Saba GK, Fraser WR, Saba VS, Iannuzzi RA, Coleman KE, Doney SC, Ducklow HW, Martinson DG, Miles TN, Patterson-Fraser DL, Stammerjohn SE, Steinberg DK, Schofield OM (2014) Winter and spring controls on the summer food web of the coastal West Antarctic Peninsula. Nat Commun 5.

Sato K, Simmonds I (2021) Antarctic skin temperature warming related to enhanced downward longwave radiation associated with increased atmospheric advection of moisture and temperature. Environ Res Lett 16:064059.

Schofield O, Brown M, Kohut J, Nardelli S, Saba G, Waite N, Ducklow H (2018) Changes in the upper ocean mixed layer and phytoplankton productivity along the West Antarctic Peninsula. Philos Trans R Soc Math Phys Eng Sci 376.

Siegel DA, Doney SC, Yoder JA (2002) The North Atlantic spring phytoplankton bloom and Sverdrup's critical depth hypothesis. Science 296:730–733.

Smith RC, Dierssen HM, Vernet M (1996) Phytoplankton biomass and productivity in the western Antarctic Peninsula region. In: *Antarctic Research Series*. Hofmann EE, Ross RM, Quetin LB (eds) American Geophysical Union, Washington, D. C., p 333–356

Stabeno PJ, Bond NA, Kachel NB, Salo SA, Schumacher JD (2001) On the temporal variability of the physical environment over the south-eastern Bering Sea. Fish Oceanogr 10:81–98.

Stabeno PJ, Kachel NB, Moore SE, Napp JM, Sigler M, Yamaguchi A, Zerbini AN (2012) Comparison of warm and cold years on the southeastern Bering Sea shelf and some implications for the ecosystem. Deep-Sea Res Part II Top Stud Oceanogr 65–70:31–45.

Stammerjohn SE, Drinkwater MR, Smith RC, Liu X (2003) Ice-atmosphere interactions during sea-ice advance and retreat in the western Antarctic Peninsula region. J Geophys Res Oceans 108:2002JC001543.

Stammerjohn SE, Martinson DG, Smith RC, Yuan X, Rind D (2008) Trends in Antarctic annual sea ice retreat and advance and their relation to El Niño-Southern Oscillation and Southern Annular Mode variability. J Geophys Res Oceans 113.

Stroeve JC, Jenouvrier S, Campbell GG, Barbraud C, Delord K (2016) Mapping and assessing variability in the Antarctic marginal ice zone, pack ice and coastal polynyas in two sea ice algorithms with implications onbreeding success of snow petrels. The Cryosphere 10:1823–1843.

Sverdrup HU (1953) On conditions for the vernal booming of phytoplankton. ICES J Mar Sci 18:287–295.

The MathWorks Inc. (2019) MATLAB version: 9.6.0 (R2019a), Natick, Massachusetts: The MathWorks Inc. https://www.mathworks.com.

Thibodeau PS, Steinberg DK, Stammerjohn SE, Hauri C (2019) Environmental controls on pteropod biogeography along the Western Antarctic Peninsula. Limnol Oceanogr 64:S240–S256.

Thomalla SJ, Racault M-F, Swart S, Monteiro PMS (2015) High-resolution view of the spring bloom initiation and net community production in the Subantarctic Southern Ocean using glider data. ICES J Mar Sci 72:1999–2020.

Tréguer P, Jacques G (1992) Dynamics of nutrients and phytoplankton, and fluxes of carbon, nitrogen and silicon in the Antarctic Ocean. Polar Biol 12.

Turner J, Maksym T, Phillips T, Marshall GJ, Meredith MP (2013) The impact of changes in sea ice advance on the large winter warming on the western Antarctic Peninsula. Int J Climatol 33:852–861.

Venables HJ, Clarke A, Meredith MP (2013) Wintertime controls on summer stratification and productivity at the western Antarctic Peninsula. Limnol Oceanogr 58:1035–1047.

Vernet M, Martinson D, Iannuzzi R, Stammerjohn S, Kozlowski W, Sines K, Smith R, Garibotti I (2008) Primary production within the sea-ice zone west of the Antarctic Peninsula: I-Sea ice, summer mixed layer, and irradiance. Deep-Sea Res Part II Top Stud Oceanogr 55:2068–2085.

Vichi M (2022) An indicator of sea ice variability for the Antarctic marginal ice zone. The Cryosphere 16:4087–4106.

965 Vives CR, Schallenberg C, Strutton PG, Boyd PW (2023) Biogeochemical-Argo floats show that
966 chlorophyll increases before carbon in the high-latitude Southern Ocean spring bloom.
967 Limnol Oceanogr Lett:lol2.10322.
968 Weinstein BG, Friedlaender AS (2017) Dynamic foraging of a top predator in a seasonal polar
969 marine environment. Oecologia 185:427–435.
970 Winder M, Sommer U (2012) Phytoplankton response to a changing climate. Hydrobiologia
971 698:5–16.
972 Xue L, Gao L, Cai W, Yu W, Wei M (2015) Response of sea surface fugacity of CO_2 to the
973 SAM shift south of Tasmania: Regional differences. Geophys Res Lett 42:3973–3979.
974 Yu L, Zhong S, Sun B (2020) The climatology and trend of surface wind speed over Antarctica
975 and the Southern Ocean and the implication to wind energy application. Atmosphere
976 11:108.
977
978

Appendix A. Notation

Abbreviation	Definition
Accumulation season	Period each year when surface chlorophyll-a concentration is increasing such that average phytoplankton mass-specific loss rates < growth rates
Chl-a	Chlorophyll-a concentration (mg m^{-3})
CMEMS	Copernicus Marine Environmental Monitoring Service
CZCS	Coastal Zone Color Scanner sensor
dChl/dt	Daily rate of change of Chl-a
ERA5	ECMWF Re-Analysis Version 5, a climate reanalysis data product generated by the European Centre for Medium-Range Weather Forecasts (ECMFW).
LTER	Long Term Ecological Research program
MERIS	Medium Resolution Imaging Spectrometer sensor
MIZ	Marginal Ice Zone
MLD	Mixed Layer Depth
MODIS-Aqua	Moderate Resolution Imaging Spectroradiometer sensor on the Aqua satellite
MODIS-Terra	Moderate Resolution Imaging Spectroradiometer sensor on the Terra satellite
OLCI-S3A	Ocean and Land Colour Instrument sensor on the Sentinel-3A satellite
OLCI-S3B	Ocean and Land Colour Instrument sensor on the Sentinel-3B satellite
OSTIA	Operational Sea Surface Temperature and Sea Ice Analysis
PAR	Photosynthetically active radiation
pCO_2	Partial pressure of carbon dioxide
Peak date	Day of year of the timing of the maximum Chl-a concentration
SAM	Southern Annular Mode
SeaWiFS	Sea-viewing Wide Field-of-view Sensor
SPF	Southern Polar Front
SST	Sea surface temperature
Start date	Day of year of the start of the phytoplankton accumulation season
SZA	Solar Zenith Angle
Threshold	Value defining bloom start date; long-term median Chl-a + 5%
VIIRS-NOAA20	Visible Infrared Imaging Radiometer Suite sensor on the NOAA-20 satellite
VIIRS-NPP	Visible Infrared Imaging Radiometer Suite sensor on the National Polar-orbiting Partnership satellite
WAP	West Antarctic Peninsula

Tables

Table 1. Regional long-term mean phenology metrics.

Ecoregion	Start date	Sd.	Peak date	Sd.	Mean Chl-a (mg m^{-3})	Sd.	Maximum Chl-a (mg m^{-3})	Sd.
Southern Polar Front	5-Sep	8	8-Dec	13	0.35	0.04	1.56	0.33
Marginal Ice Zone	18-Oct	21	17-Dec	21	0.61	0.14	2.87	0.69
Northern Shelf	13-Nov	8	22-Jan	13	0.84	0.21	3.57	1.03
Mid Shelf	13-Dec	11	29-Jan	10	1.24	0.34	5.34	1.66
Southern Shelf	2-Jan	6	12-Feb	9	1.47	0.54	6.01	2.76

Sd. indicates standard deviation. Standard deviations of start date, and peak date are in units of days. Standard deviations of mean and maximum Chl-a are in units of mg m^{-3}.

Table 2. Decadal medians and differences between decades for regionally averaged phenology indices.

Ecoregion	Start Date				Peak Date			
	Median 2001-11	Median 2012-22	Difference (days)	p	Median 2001-11	Median 2012-22	Difference (days)	p
Southern Polar Front	3-Sep	1-Sep	-2	0.880	5-Dec	17-Dec	12	0.257
Marginal Ice Zone*	9-Oct	26-Oct	17	0.016*	7-Dec	5-Jan	29	0.003*
Northern Shelf*	10-Nov	20-Nov	10	0.010*	17-Jan	2-Feb	16	0.034*
Mid Shelf*	7-Dec	26-Dec	19	0.013*	20-Jan	11-Feb	22	0.059
Southern Shelf	27-Dec	9-Jan	13	0.151	9-Feb	16-Feb	7	0.364

* Trends were statistically significant (Kruskal-Wallis; $p < 0.05$).

996
997 **Table 3.** Trends in regionally averaged phenology indices.

Ecoregion	Start date		Peak date	
	Trend (d yr^{-1})	p	Trend (d yr^{-1})	p
Southern Polar Front*	-0.435	0.293	1.048	0.007*
Marginal Ice Zone*	0.595	0.141	1.548	0.018*
Northern Shelf	0.381	0.293	0.429	0.293
Mid Shelf	0.848	0.118	1.037	0.183
Southern Shelf	0.679	0.154	0.434	0.559

998 * Statistically significant trends (Mann-Kendall; $p < 0.05$).
999
1000 **Table 4.** Trends in regionally averaged, de-seasonalized monthly Chl-a.

Ecoregion	Monthly Chl-a		
	Trend (mg m^{-3} yr^{-1})	Relative trend (% yr^{-1})	p
Southern Polar Front*	0.00007	0.02	0.0004*
Marginal Ice Zone	-0.00002	-0.003	0.743
Northern Shelf	-0.00007	-0.01	0.198
Mid Shelf	-0.00009	-0.009	0.355
Southern Shelf	-0.0001	-0.009	0.227

1001 * Statistically significant trends (Mann-Kendall; $p < 0.05$).
1002

Figures

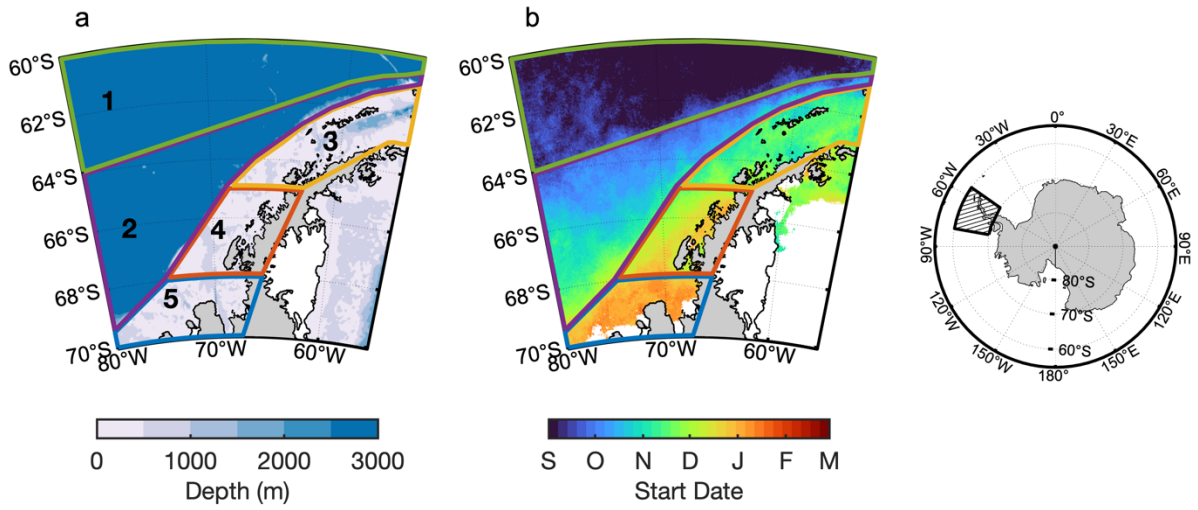

Fig. 1. Map of the West Antarctic Peninsula with regions overlaid on a) bathymetry and b) mean start date of the phytoplankton accumulation season 1997-2022. Months indicate the first day of each month (e.g., "S" = September 1). Regions include 1. Southern Polar Front, 2. Marginal Ice Zone, 3. Northern Shelf, 4. Mid Shelf, and 5. Southern Shelf. Gray indicates land, white indicates ice shelves. In b) non-ice shelf areas that are colored white correspond with satellite data where <30% of daily scenes were present due to frequent presence of sea ice.

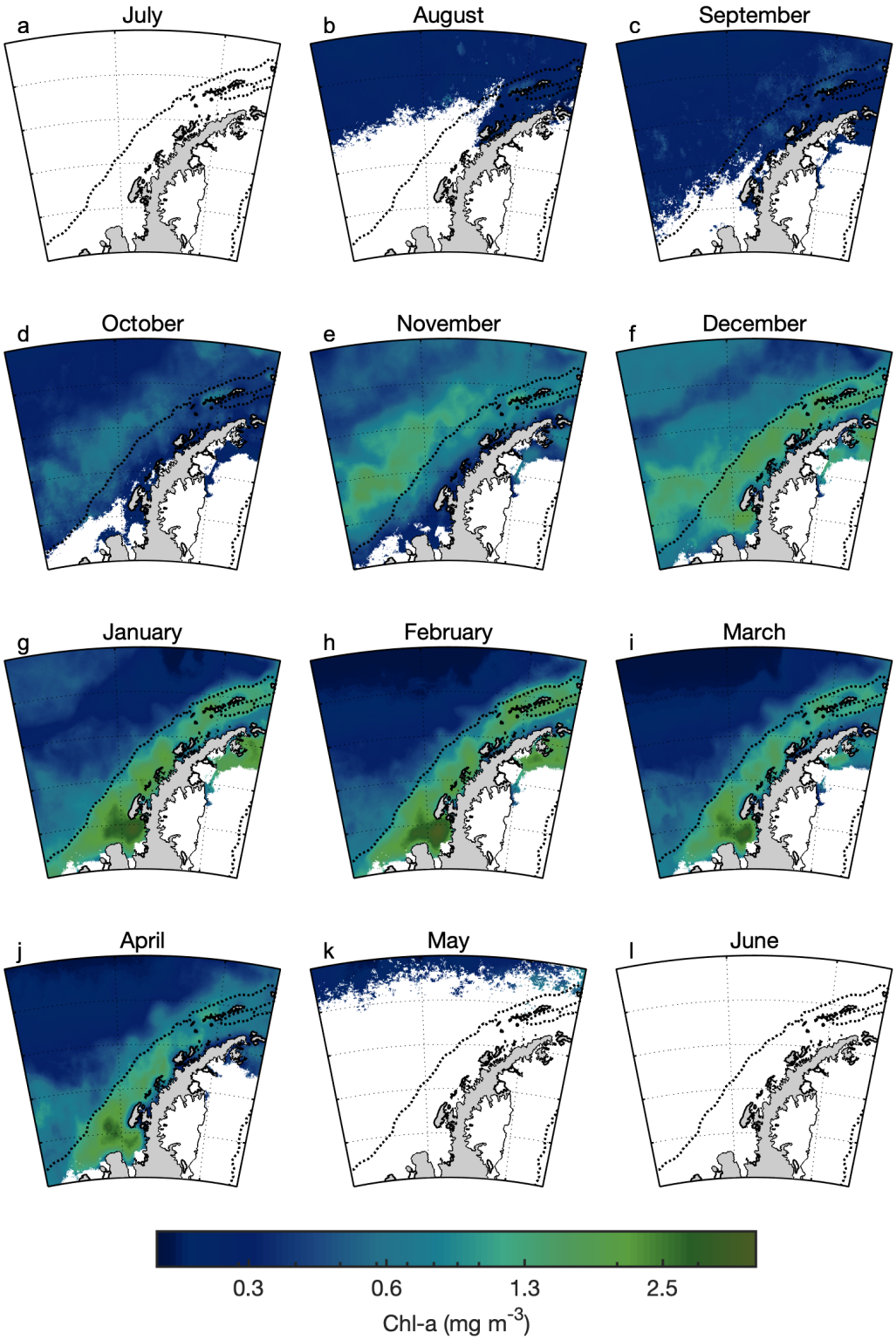

Fig. 2. Monthly climatologies of Chl-a, showing the average of 1997-2022 for each month. Climatologies were calculated for spatial points where >75% of data were available (>18 of 24 years). White space in some months indicates where satellite data are unavailable due to sea ice and low light. Black dotted line indicates the continental shelf break (1000 m isobath).

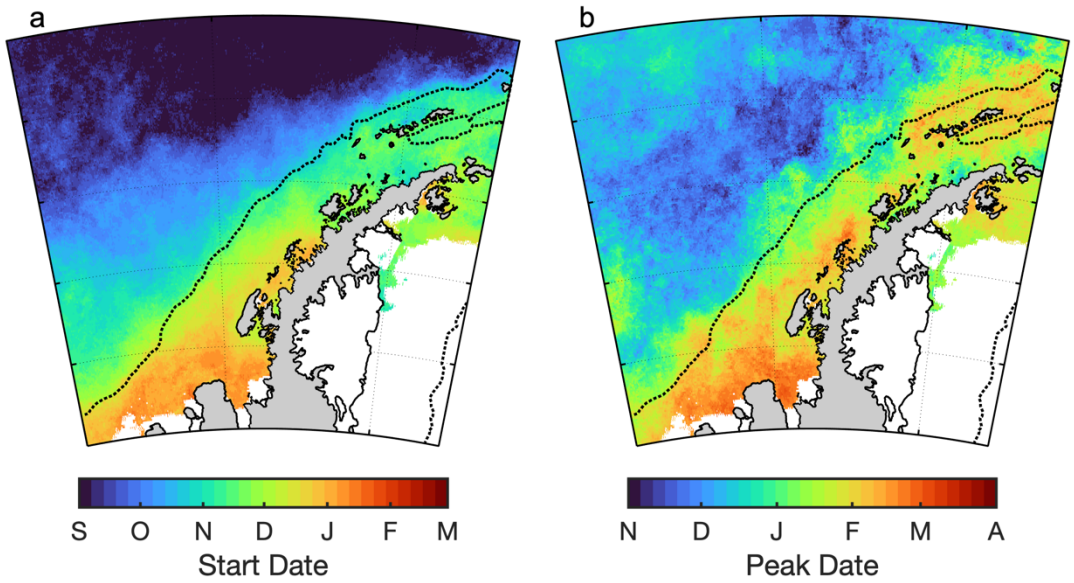

Fig. 3. Long-term mean bloom indices: a) start date of the phytoplankton accumulation season via the threshold method, b) peak date (date of maximum chl-a concentration). Lettering on colorbars indicates the first day of each month (e.g., S = September 1st). Black dotted line indicates the continental shelf break (1000 m isobath).

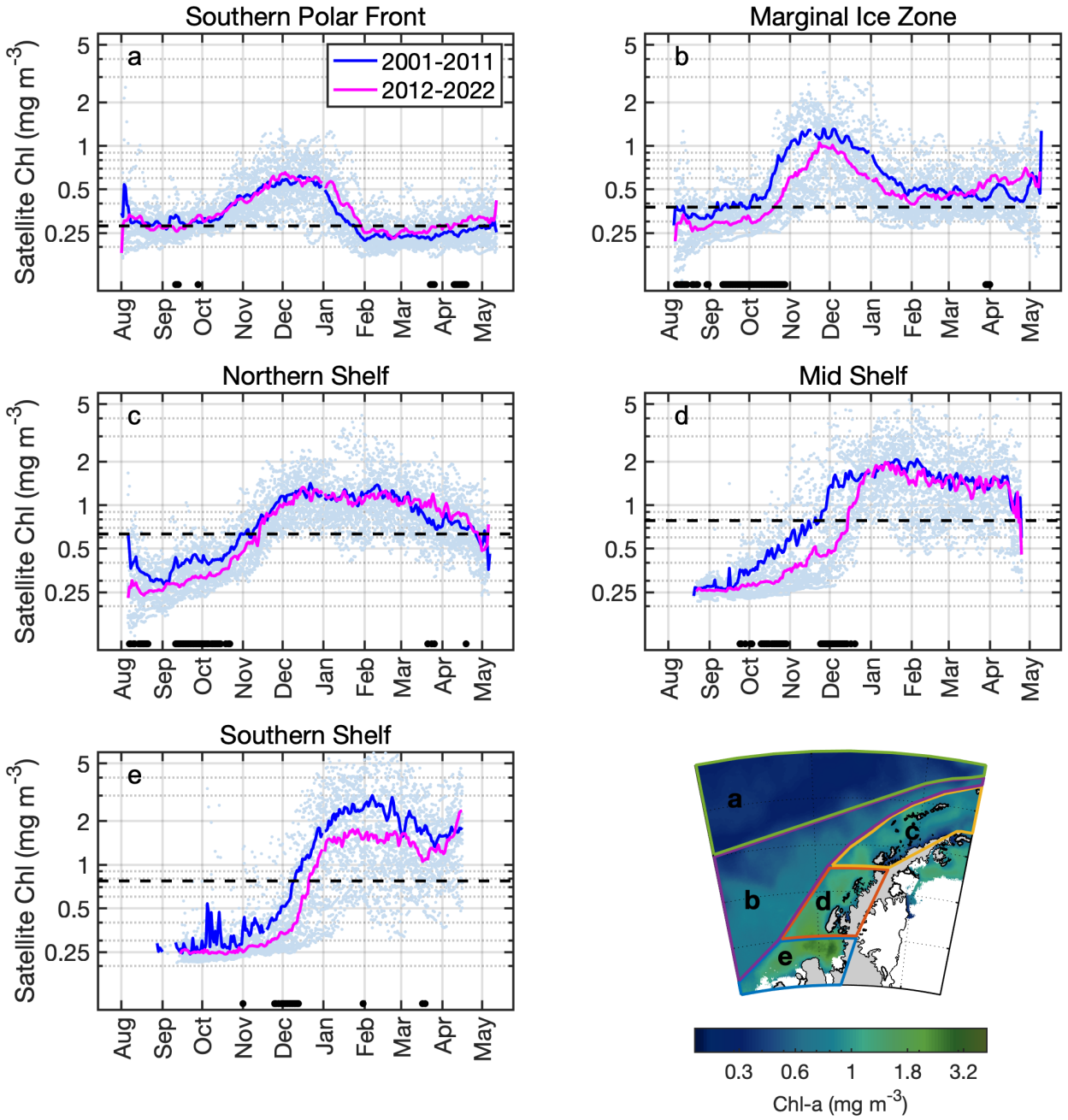

Fig. 4. Seasonal cycles of daily Chl-a concentration for two decades 2001-2011 (blue) vs. 2012-2022 (magenta). Dotted black line indicates the threshold value (long term median Chl-a + 5%) for each region used to calculate start date. Black circles at lower edges of plots indicate where the difference between decades was statistically significant (Kruskal-Wallis test, $p < 0.05$). Dates refer to the 1st of each month (e.g., "Aug" is 1 August). Regions shown in map inset overlay long-term mean Chl-a concentration.

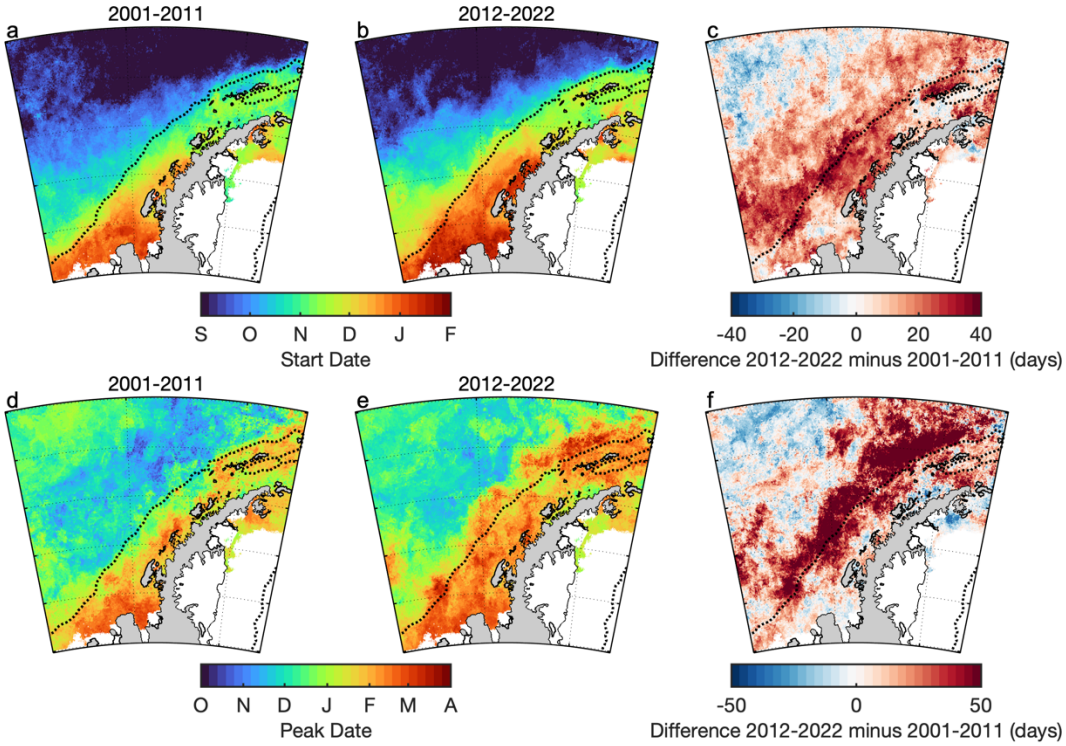

Fig. 5. Decadal mean start dates, peak dates, and decadal differences (days). a) Mean start date 2001-2011, b) mean start date 2012-2022, c) difference 2012-2022 mean start date minus 2001-2011 mean start date, d) mean peak date 2001-2011, e) mean peak date 2012-2022, and f) difference 2012-2022 mean peak date minus 2001-2011 mean peak date (days). In c) and f) blue indicates earlier start date and red indicates later dates in recent years compared to the earlier decade. Black dotted line indicates the continental shelf break (1000 m isobath).

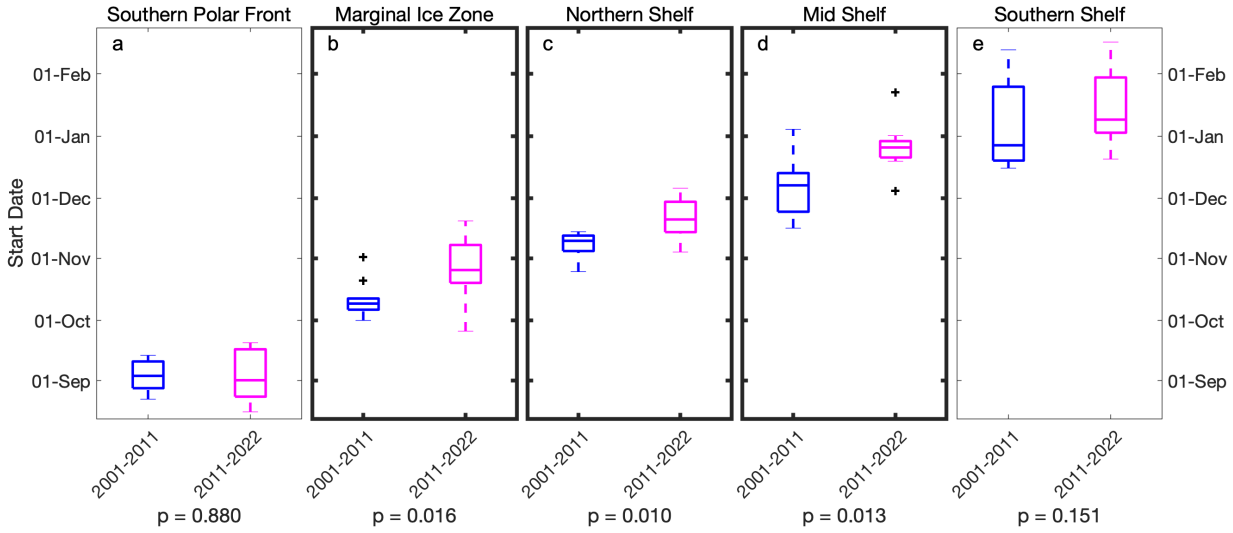

Fig. 6. Median start dates by ecoregion for 2001-2011 (blue) and 2012-2022 (magenta) for a) southern polar front, b) marginal ice zone, c) northern shelf, d) mid shelf, and e) southern shelf. On each box, the central mark is the median, the edges of the box are the 25th and 75th percentiles, black crosses indicate outliers. Bolded plot outlines indicate ecoregions where decadal differences were statistically significant and p values are given via Kruskal-Wallis tests.

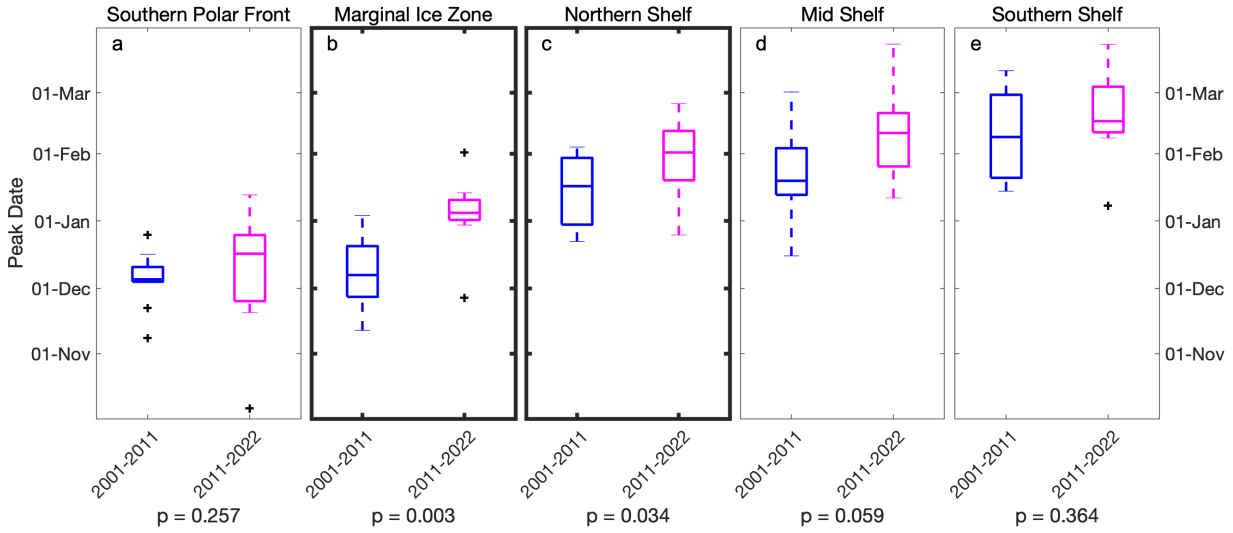

Fig. 7. Median peak dates by ecoregion for 2001-2011 (blue) and 2012-2022 (magenta) for a) southern polar front, b) marginal ice zone, c) northern shelf, d) mid shelf, and e) southern shelf. On each box, the central mark is the median, the edges of the box are the 25th and 75th percentiles, and black crosses indicate outliers. Bolded plot outlines indicate ecoregions where decadal differences were statistically significant and p values are given via Kruskal-Wallis tests.

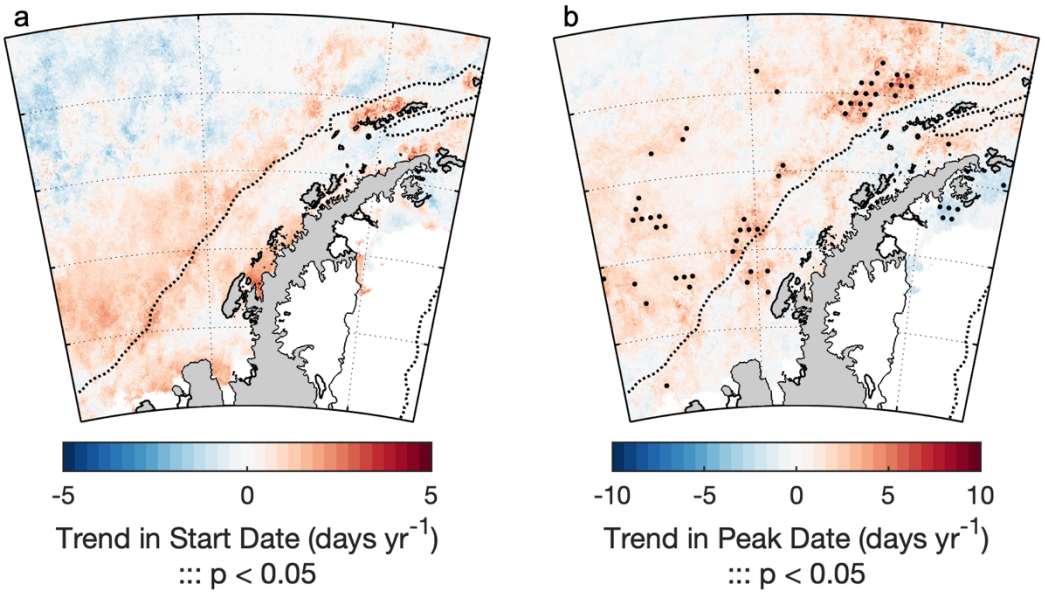

Fig. 8. Trends in a) start date and b) peak date of the phytoplankton accumulation season per season over time, in units of days per year (Theil-Sen slope). Red indicates a later date over time while blue indicates an earlier date over time. Black stippling indicates areas where trends are statistically significant ($p < 0.05$; Mann-Kendall). Black dotted line indicates the continental shelf break (1000 m isobath).

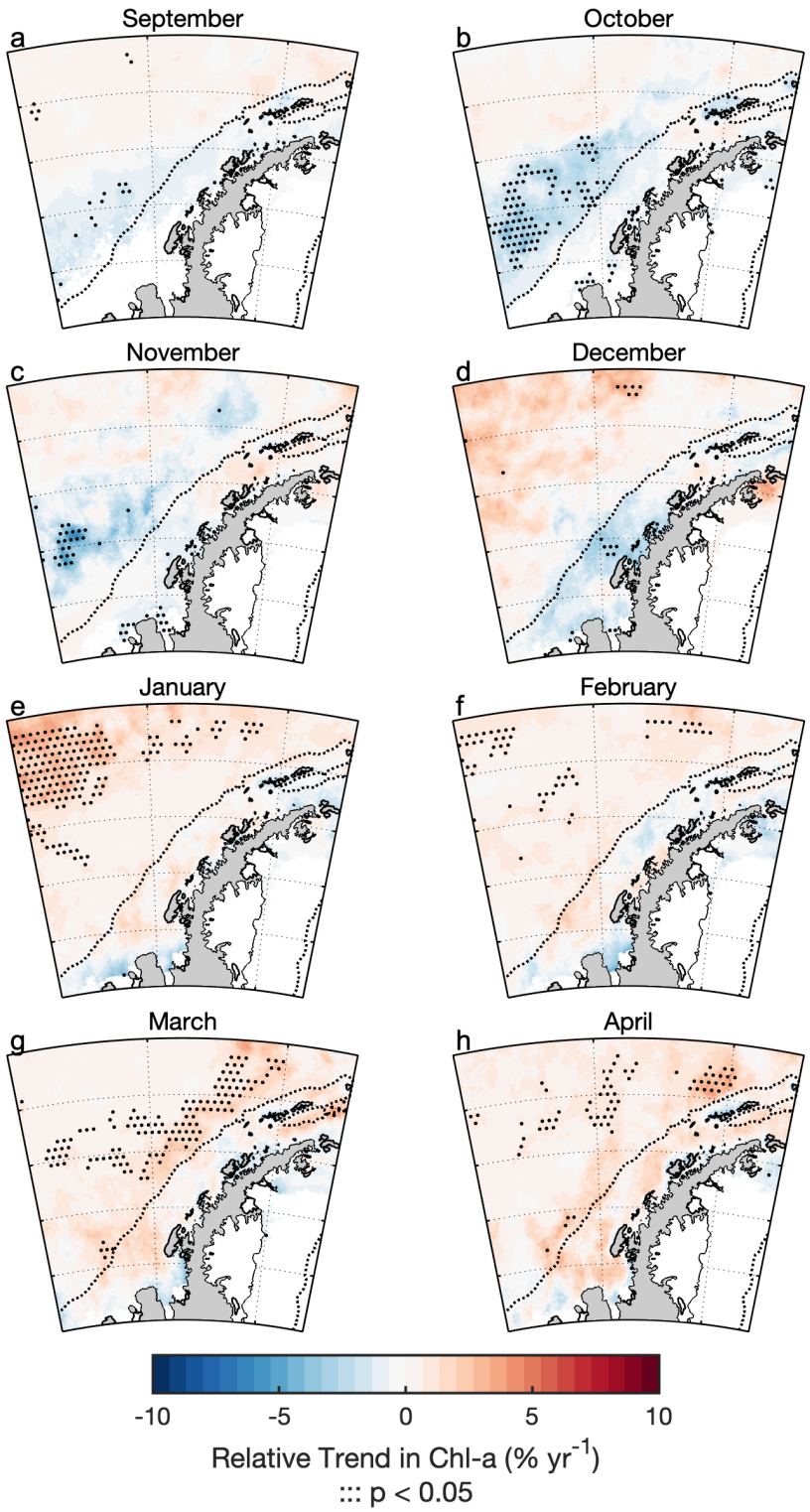

Fig. 9. Trends in Chl-a by month relative to the long-term mean Chl-a for each spatial point for each month over the 25-year time series (Theil-Sen slope). Black stippling indicates areas where trends are statistically significant ($p < 0.05$; Mann-Kendall). Black dotted line indicates the continental shelf break (1000 m isobath).

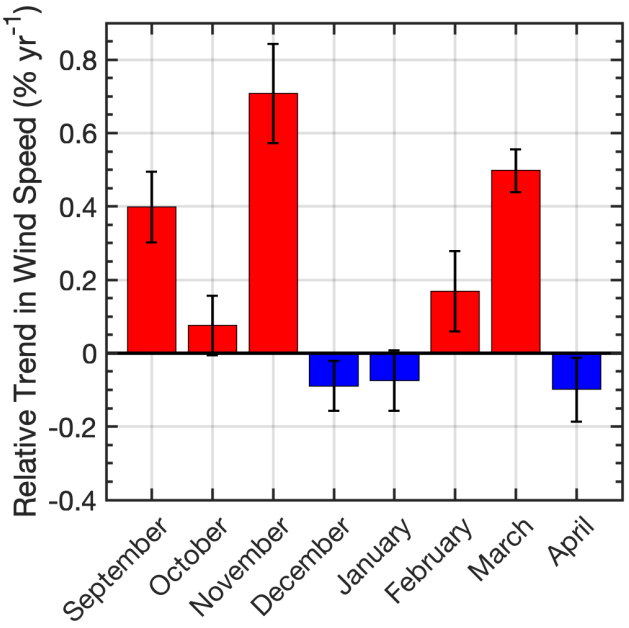

Fig. 10. Relative trends in wind speed by month averaged for the southern polar front (SPF) ecoregion 1997-2022 from ERA5 (Theil-Sen slope). Relative trends were normalized to the long-term mean wind speed at each x,y location for each month. Error bars indicate spatial standard deviation of trends over time.

1081

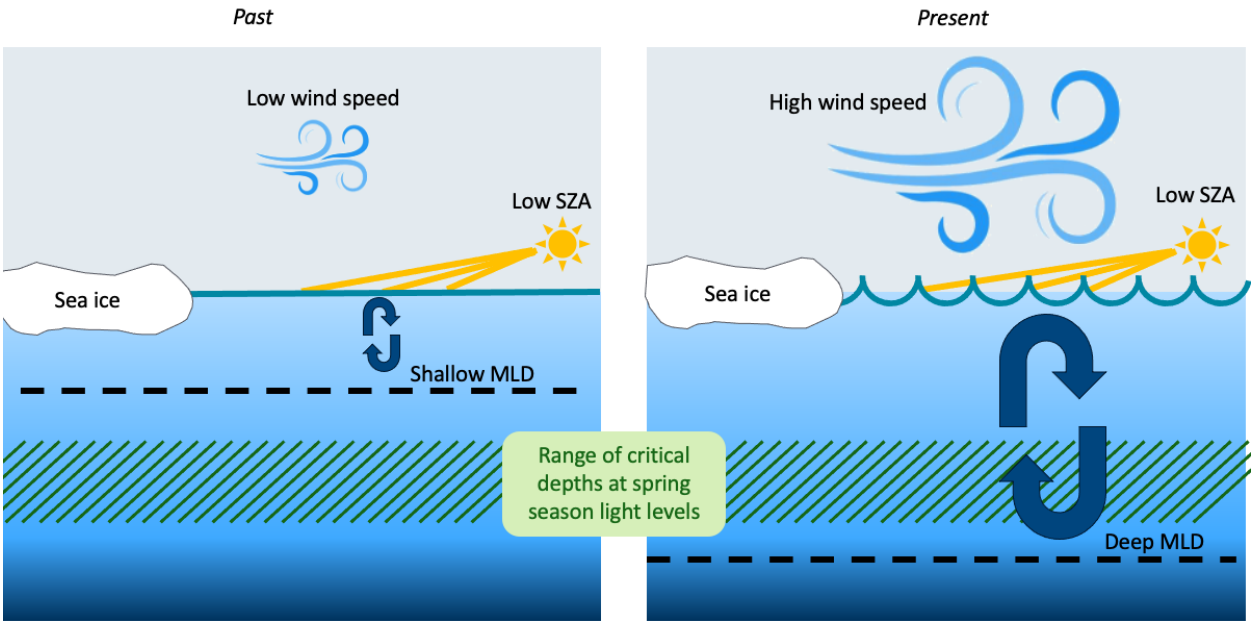

1082
1083 **Fig. 11.** Conceptual diagram illustrating past conditions vs. present conditions in the marginal ice
1084 zone west of the Antarctic Peninsula in the spring season (October to November). Spring
1085 conditions are inherently light limited due to low solar zenith angles (SZA). Past conditions with
1086 lower wind speeds and shallower mixed layer depth (MLD) provided more favorable conditions
1087 for spring surface phytoplankton accumulation compared to present conditions.
1088